

## Modelling Scenarios for KEM-15 (“Cooling induced seismicity”)

*Prepared by: Hannes Hofmann, Günter Zimmermann (GFZ Potsdam)*

*Reviewed by: Arno Zang (GFZ Potsdam), Serge Shapiro (FU Berlin)*

3 November 2023

This document contains a list of data and numerical simulation scenarios of cooling induced seismicity using the Finite Element Code GOLEM (Jacquey and Cacace, 2017). The model is based on the published and history matched GOLEM model of Groß Schönebeck Enhanced Geothermal System in a Rotliegend reservoir (Blöcher et al., 2018). This model is adapted for conditions in the Netherlands. As of 1 January 2019, 24 geothermal systems were in operation in the Netherlands (Mijnlieff, 2020). The three most relevant geothermal plays are subject to this numerical modelling study:

- **Hot sedimentary aquifer above Zechstein in 1.5-3.0 km depth (Upper Jurassic play, Delft Sandstone)**

Nine geothermal doublets are installed in the Delft sandstone (as of 22 Feb 2019; Mijnlieff, 2020).

- **Hot sedimentary aquifer below Zechstein in 1.5-3.0 km depth (Rotliegend play, Slochteren Sandstone)**

Eight geothermal projects currently exploit the Slochteren sandstone (as of 22 Feb 2019; Mijnlieff, 2020).

- **Petrothermal reservoir below 3.0 km depth (Dinantian limestone)**

Two geothermal systems currently exist in Dinantian limestone that rely on fracture permeability. For both geothermal systems, the production well is in a faulted/fractured Dinantian limestone sequence in or close to the Tegelen fault. The positions of the injection locations are away from the fault, perpendicular to the fault trace, into karstified fractured and possibly faulted limestone. However, no Enhanced Geothermal System exists currently in the Netherlands (Mijnlieff, 2020).

Parameters indicated in this document are based on the geological understanding and geological literature/data analysis presented in the internal KEM-15 project report “WP1 Geological review study”) and represent already synthesized values used for the numerical models. These parameters are the basis of different modelling scenarios described here.

Scenarios for a sensitivity analysis are setup for the Slochteren Sandstone model. For the Delft sandstone model and Dinantian limestone model no sensitivity analysis will be performed. Instead, representative modelling scenarios will be setup. Simulation results are described in separate reports.

# 1. Slochteren Sandstone

This section describes the hydrothermal reservoir properties below the Permian salt in the Netherlands. The considered reservoir formation is the Slochteren Sandstone Formation which is part of the Upper Rotliegend Group. The Zechstein Group is simplified to one homogeneous rock salt formation and used as the top layer. The Carboniferous (Limburg Group) is approximated as one homogeneous claystone and is used as the bottom layer. For each of the values the corresponding reasoning and reference is given. If no reference is provided, an estimate is made based on expert knowledge. We are interested in the effect of geothermal operations on a single fault. Thus, we include only one fault in the model, which is approximated as a planar two-dimensional discontinuity in a three-dimensional rock matrix.

Conceptually, we thus simplify the geology to a conceptual model consisting of a horizontal rock salt layer (Zechstein Group) as top seal, a horizontal sandstone layer (Slochteren formation) as reservoir unit and a horizontal claystone layer (Limburg Group) as basement. All layers are intersected by a single inclined fault (Figure 1). No fault offset is assumed. Hot water production and cold-water injection is modelled through a typical Dutch geothermal well doublet. Both wells are vertical and intersect the entire Slochteren reservoir. As mostly the entire reservoir section is accessed, the wells are assumed to be open to flow along the entire well path inside the Slochteren formation.

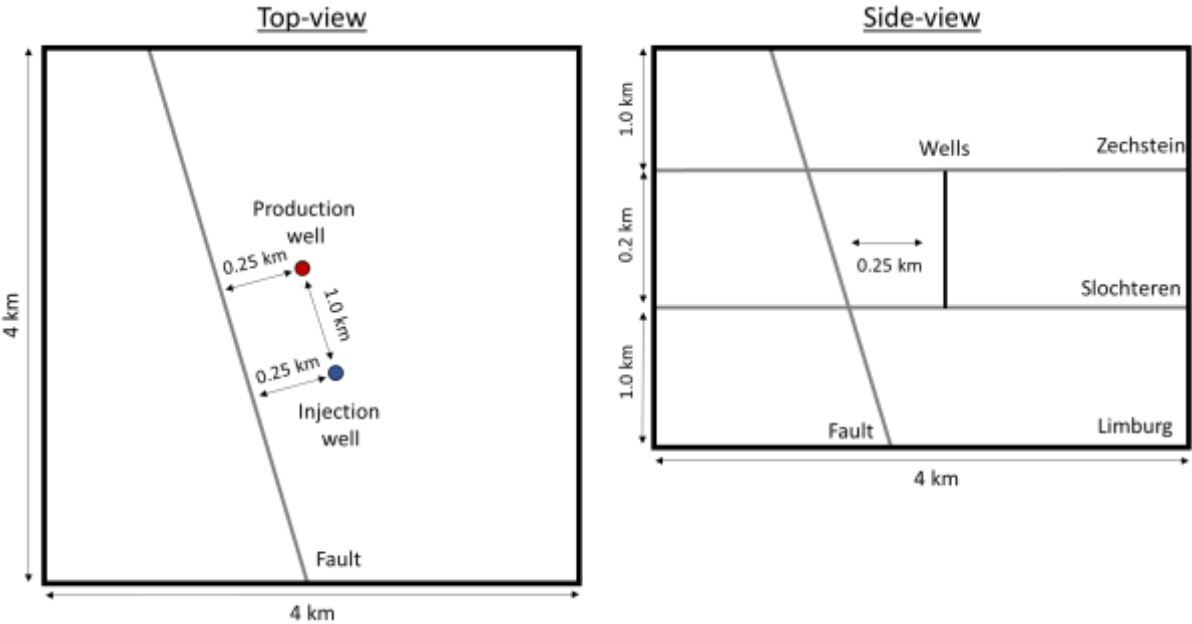


Figure 1: Conceptual numerical model setup for the Slochteren reservoir. Distances represent the base case scenario (not to scale).

## 1.1. Data summary

### 1.1.1. Geological model geometry

The **top** of the **Rotliegend** reservoir varies between 1500 m and 3000 m (Mijnlieff, 2020). We chose the Middenmeer site with a top Rotliegend depth of 2200 m (<http://www.destress-h2020.eu/en/demonstration-sites/middenmeer>) as representative for the base case model. According to Mijnlieff (2020) the **thickness** of the **Rotliegend** reservoir varies between 100 m and 250 m. Again, we chose the Middenmeer site with a thickness of 200 m as representative for the base case model (<http://www.destress-h2020.eu/en/demonstration-sites/middenmeer>).

The **thickness** of the overlying **Zechstein** group varies between <100 m (in marginal settings) and >1200 m (in the salt basin; TNO-GSN, 2021a, Duin et al., 2006). According to the thickness map of the Zechstein Group in Duin et al. (2006), 200 m can be considered as a typical Zechstein thickness in the area of current geothermal operations in the Rotliegend group. The range of **Zechstein tops** in Table 1 is based on the Rotliegend top range and Zechstein thickness of 200 m.

Even though the **Limburg** group has typically a **thickness** of ~600 m, which can reach up to 1300 m (<https://www.dinoloket.nl/en/subsurface-models>), we use a thickness of only 200 m for the Limburg group in our simulations to reduce model runtimes. The **Limburg top** range in Table 1 results from the minimum and maximum unit top and unit thickness of the Rotliegend.

For this modeling exercise we are interested in the effect of geothermal operations on large-scale (regional) faults that can potentially host larger magnitude seismic events. Structural element directions and fault patterns are relatively homogeneous across the whole onshore part of the Netherlands with a main **fault trend** varying from NW-SE to NNW-SSE (maps in Duin et al., 2006; de Jager, 2007). We do not consider secondary fault systems, that strike in different directions. We recommend investigating the impact of secondary order fault systems in future studies. This is because orthogonal fracture and fault networks can cause larger seismic events by fracture interaction processes. Fracture intersection is usually not covered in single fault, or multiple isolated fault systems. The superposition principle is invalid to apply. An example for stress variability in systems with interacting and intersecting faults is given in Yoon and Zang 2019. According to the figures in de Jager (2007) these faults may dip in different directions. However, we consider only a **dip** towards NE. Cross-sections in de Jager (2007) show that most faults are sub-vertical. Thus, we assume a typical fault dip of 80°, which may vary between 60 and 85°.

*Table 1: Model geometry data. For the numerical model the faults are assumed to intersect all three layers and extend laterally through the entire model since fault lengths are estimated to be >10 km based on de Jager (2007). A typical fault spacing of ~5 km (de Jager, 2007) warrants using a single fault only in the models.*

Model property	Zechstein (rock salt)	Rotliegend (sandstone)	Limburg (claystone)
Unit top (m)	2000 <sup>1</sup> (1300 <sup>1</sup> -2800 <sup>1</sup> )	2200 <sup>3</sup> (1500-3000) <sup>4</sup>	2400 <sup>1</sup> (1600 <sup>1</sup> -3250 <sup>1</sup> )
Unit thickness (m)	200 <sup>1</sup> (<100 <sup>2</sup> ->1200 <sup>2</sup> )	200 <sup>3</sup> (100-250) <sup>4</sup>	200 <sup>1</sup> (up to 1300 <sup>5</sup> )
Fault strike	N130°E <sup>1,6</sup> (N150°E <sup>1,6</sup> )	N130°E <sup>1,6</sup> (N150°E <sup>1,6</sup> )	N130°E <sup>1,6</sup> (N150°E <sup>1,6</sup> )

Fault dip (° from horizontal)	80 <sup>6</sup> (60-85) <sup>6</sup>	80 <sup>6</sup> (60-85) <sup>6</sup>	80 <sup>6</sup> (60-85) <sup>6</sup>
Fault dip direction	NE <sup>6</sup>	NE <sup>6</sup>	NE <sup>6</sup>

<sup>1</sup>Duin et al. (2006), <sup>2</sup>TNO-GSN (2021a), <sup>3</sup><http://www.destress-h2020.eu/en/demonstration-sites/middenmeer>, <sup>4</sup>Mijnlieff (2020), <sup>5</sup>TNO-GSN (2021b), <sup>6</sup>de Jager (2007)

### 1.1.2. Stress, pressure and temperature data

A **heat flow** of 70 mW/m<sup>2</sup> is assumed according to Bonté et al. (2014).

The average **temperature gradient** in the Netherlands can be considered as 31°C/km with a surface temperature of 10°C and an uncertainty of  $\pm 10^\circ\text{C}$  (Bonté et al., 2014). We therefore use 31°C/km+10°C for the base case, 20°C/km+10°C as minimum temperature gradient and 40°C/km+10°C as maximum temperature gradient.

Despite the possibility of local fluid overpressures (Verweij et al., 2012), we assume a hydrostatic **pore pressure gradient** in our simulations. The hydrostatic pore pressure gradient depends on the density of the water. We assume a minimum density of 1020 kg/m<sup>3</sup> (representative for seawater) and a maximum density of 1220 kg/m<sup>3</sup> (representative for a brine with salinity of ~400 g/l). This corresponds to minimum and maximum pore pressure gradients of 10 and 12 MPa/km. For the base case scenario, we chose 11 MPa/km, representative for the Groß Schönebeck geothermal site with 265 g/l salinity (Blöcher et al., 2010). Formation water salinity typically increases with depth and rarely reaches values above 400 g/l in the Dutch Rotliegend (Veldkamp et al., 2016).

We assume a normal **faulting regime** (SV>SHmax>Shmin) according to Guises et al. (2015), who performed a geomechanical modeling study of the Groningen gas field.

According to Verweij et al. (2016) the **vertical stress gradient** in the Netherlands is frequently below the standard gradient of ~23 MPa/km (corresponding to ~2300 kg/m<sup>3</sup> bulk density). However, in the West Netherlands Basin a standard gradient is observed (Verweij et al., 2016). Van Eijs (2015) shows vertical stress gradients increasing with depth from ~19-21 MPa/km at 1 km depth to 22-24 MPa/km (at 3 km depth). We therefore assume a vertical stress gradient of 22 MPa/km for the base case scenario with a possible variation between 21 MPa/km and 23 MPa/km. Note, that these are average gradients over the entire depth range and only the corresponding effective horizontal stress values at the center of the Slochteren formation are matched in the model. The actual stress gradients in the individual layers depend on the elastic rock properties.

According to TNO (2015), the standard **minimum horizontal stress gradient** can be considered as 0.6 times the standard vertical gradient of 23 MPa/km ( $\Delta\text{Shmin}=13.8$  MPa/km). They find that the leak-off pressure, which is representative for the minimum horizontal stress, is rarely below this standard gradient and is also bound by the lithostatic stress gradient. Osinga and Buik (2019) propose a Shmin gradient of 18 MPa for the deeper Dinantian formation. Guises et al. (2015) determined minimum horizontal stress gradients of 15.4-16.7 MPa/km for the Groningen gas field. We assume a minimum horizontal stress gradient of 14 MPa/km for the base case scenario with 13 MPa/km and 20 MPa/km as lower and upper bound of the minimum horizontal stress gradient. The upper bound results from the assumption that the minimum horizontal stress is never larger than the maximum horizontal stress. We therefore assume that the faulting regime is always a normal faulting regime with possible transition to strike slip (when SHmax and Shmin are equal).

According to van Eijs (2015), a relatively low difference between the minimum and **maximum horizontal stress gradients** is found in the Groningen gas field. Different methods yield a variation of the ratio SHmax/Shmin between 1.02 and 1.42. Osinga and Buik (2019) propose that SHmax is ~5-20% higher than Shmin as a good starting assumption when data is lacking. Guises et al. (2015) determined maximum horizontal stress gradients of 17.3-18.2 MPa/km for the Groningen gas field. We assume a typical SHmax/Shmin ratio of 1.07 for the base case scenario ( $\Delta SH_{max}=1.07*14 \text{ MPa/km}=15 \text{ MPa/km}$ ), a lower bound for the SHmax gradient equal to the minimum horizontal stress gradient (14 MPa/km) and an upper bound of the SHmax gradient equal to 20 MPa ( $\Delta SH_{max}=1.42*14 \text{ MPa/km}=20 \text{ MPa/km}$ ). Note that SHmax has the largest uncertainty among all stress magnitudes.

According to Mechelse (2017), the pre- and post-salt stress directions are similar.

The **maximum horizontal stress direction** in the Netherlands is typically NW-SE with values ranging between N130°E and N5°E (Heidbach et al., 2016). Guises et al. (2015) determined the maximum horizontal stress direction to be N160°E in the Groningen gas field. We assume N160°E for the base case scenario and a typical range between N150°E and N170°E for the sensitivity analysis (Table 2). Note that stress directions may strongly vary locally since stress rotations can be expected near salt domes and fault zones, which we do not consider in our sensitivity analysis. As a rule of thumb, the distance from heterogeneity (dome, fault) needs to be five times the size of the heterogeneity before obstacle-induced stress variations become insignificant (Zang and Stephansson, 2010). This rule-of-thumb does not hold for intersecting faults.

*Table 2: Stress, pressure and temperature data. Note that both horizontal stress gradients equal to the vertical stress gradient in the Zechstein layer.*

<b>Model property</b>	<b>Value</b>
Heat flow	70 mW/m <sup>2</sup> <sup>1</sup>
Temperature gradient	31°C/km (20-40°C/km) + 10°C <sup>1</sup>
Pore pressure gradient	11 MPa/km (10-12 MPa/km) <sup>2</sup>
Vertical stress gradient	22 MPa/km (21-23 MPa/km) <sup>3</sup>
Maximum horizontal stress gradient	15 MPa/km (14-20 MPa/km) <sup>4</sup>
Minimum horizontal stress gradient	14 MPa/km (13-20 MPa/km) <sup>3</sup>
Maximum horizontal stress direction	N160°E (N150°E-N170°E) <sup>5</sup>

<sup>1</sup>Bonté et al. (2012), <sup>2</sup>Verweij et al., 2012, <sup>3</sup>TNO (2015), <sup>4</sup>van Eijs (2015), <sup>5</sup>Heidbach et al. (2016) and Mechelse (2017)

### 1.1.3. Geomechanical properties

The elastic model properties are summarized in

*Table 3.* Zhang et al. (2018) find that rock salt may actually show poromechanical behavior, which they characterized in laboratory experiments. They find that the Biot coefficient of rock salt is in the order of 0.2-0.3. Missal (2019) report that the Biot coefficient of intact rock salt is ~0.4, of damaged rock salt is ~1 and that the in-situ Biot coefficient of rock salt is 0.12 according to Kansy (2007).

Malkowski et al. (2012) determined Young's moduli of ~10 GPa for Carboniferous rocks.

The Slochteren reservoir sandstone primarily consists of quartz. According to Schmitt (2015) the solid bulk modulus of Quartz is 37.8 GPa ( $\alpha$ -Quartz) and 42.97 GPa ( $\beta$ -Quartz). The Zechstein group may consist of Halite, Anhydrite, Calcite and Dolomite. The solid bulk modulus of Calcite, Dolomite, Anhydrite and Halite is 73.3 GPa, 94.9 GPa, 54.9 GPa and 24.9 GPa, respectively (Schmitt, 2015). Claystones, which we assume representative for the Carboniferous in our model, primarily consist of Illite, Smectite (Montmorillonite) and Kaolinite. The solid bulk modulus of Muscovite, dry Na Montmorillonite, wet Montmorillonite and Kaolinite is 58.2 GPa, 82 GPa, 36 GPa, and 71.1 GPa, respectively.

Lele et al. (2015) performed a geomechanical modeling study of the Groningen gas field. For the **Zechstein** Halite they use a **Young's modulus** (E) of 30 GPa and a **Poisson's ratio** ( $\nu$ ) of 0.35 while they use a Young's modulus of 40 GPa and a Poisson's ratio of 0.2 for the Carboniferous.

We use the same parameters for the base case model in our study except for the Poisson's ratio of the Zechstein, where we used 0.3 for consistency with the Biot coefficient  $\alpha$  (otherwise  $\alpha$  would be below 0). Using a **solid bulk modulus**  $K_s$  of 30 GPa, this yields a **Biot coefficient** of 0.17, consistent with a low-porosity rock salt formation. The Biot coefficient of the **Limburg** group is difficult to assess. We assumed a solid bulk modulus of 50 GPa, representative for clay according to Delage (2013). This yields a Biot coefficient of 0.56 for the Limburg group, which we assume to be a claystone. Both elastic properties of the Zechstein and Limburg groups may vary significantly depending on the local mineralogical composition.

For the **Rotliegend** reservoir Lele et al. (2015) use a porosity dependent **Young's modulus** and **Poisson's ratio** with values of 10 GPa and 0.18 at 20% porosity and a variation between 1 GPa and 35 GPa and between 0.05 and 0.25. Zang et al. (1996) determined the Young's modulus of several Flechtingen Sandstone samples and found values between 14 GPa and 29 GPa for dry samples and between 12 GPa and 24 GPa for wet samples. Pijenburg et al. (2019) determined Young's moduli between 3 and 22 GPa for Slochteren Sandstone depending on the porosity and the effective confining pressure. They also find typical values for Poisson's ratio close to 0.2. Lele et al. (2015) report values of **Biot's coefficient** between 0.5 and 1 and a Biot coefficient of close to 0.9 for 20% porosity. We therefore assume base case values of  $E=10$  GPa,  $\nu=0.2$  and  $\alpha=0.86$  with upper and lower bounds between 3 and 30 GPa for Young's modulus, 0.1 and 0.25 for Poisson's ratio and 0.5 and 0.97 for Biot's coefficient.

Biot coefficient  $\alpha$  is calculated based on drained bulk modulus  $K = \frac{E}{3(1-2\nu)}$  (with Young's modulus E and Poisson's ratio  $\nu$ ) and solid bulk modulus  $K_s$  (measured):  $\alpha = 1 - \frac{K}{K_s}$ . Using these formulas, we determined the drained bulk modulus and the Biot coefficient in

*Table 3* and checked all values for internal consistency and consistency with literature values. We

assume a solid bulk modulus of 40 GPa for the Rotliegend sandstone in all our models.

Table 3: Elastic properties of all model units.

Model property	Zechstein (rock salt)	Rotliegend (sandstone)	Limburg (claystone)
Young's modulus (GPa)	30 <sup>1</sup>	15 (3-30) <sup>1,2</sup>	40 <sup>1</sup>
Poisson's ratio (-)	0.3 <sup>1</sup>	0.2 <sup>1,2</sup> (0.1-0.25) <sup>1,2</sup>	0.2 <sup>1</sup>
Solid bulk modulus (GPa)	30 <sup>3</sup>	40 <sup>3</sup>	50 <sup>5</sup>
Drained bulk modulus* (GPa)	25	8.33 (1.3-20)	22.2
Biot coefficient* (-)	0.17	0.86 <sup>1,4</sup> (0.5-0.97) <sup>1,4</sup>	0.56

<sup>1</sup>Lele et al. (2015), <sup>2</sup>Pijnenburg et al. (2019), <sup>3</sup>Schmitt (2015), <sup>4</sup>Trautwein (2005), <sup>5</sup>Delage (2013),  
\*calculated

#### 1.1.4. Hydraulic properties

The (**horizontal**) permeability of the exploited **Rotliegend** reservoirs is between 50 and 350 mD according to Mijnlief (2020). Given that a minimum transmissivity (permeability\*thickness) of 10-15 Dm is required for a successful project (Mijnlief, 2020) and a typical thickness of 200 m, we assume 100 mD as a representative base case scenario with 20 Dm transmissivity. However, the **vertical permeability** is typically 2 to 10 times lower compared to the horizontal permeability (e.g., Doddema, 2012; Mohammed, 2020). We use a ratio between horizontal and vertical permeability of 2 for the base case scenario and a range between 1 and 10. According to Lele et al. (2015) and Pijnenburg et al. (2019) Rotliegend sandstone **porosity** may range approximately between 10 and 30 %. We use 20% for the base case scenario (Table 4).

Both **Zechstein** rock salt and **Limburg** claystone can be considered as nearly impermeable formations. Therefore, we assume a **horizontal and vertical permeability** of 0.001 mD and a **porosity** of 1% for both formations.

Table 4: Hydraulic properties of all model units.

Model property	Zechstein (rock salt)	Rotliegend (sandstone)	Limburg (claystone)
Hor. permeability (mD)	0.001	100 (50-350) <sup>1</sup>	0.001
Hor./vert. permeability (-)	1	2 (1-10) <sup>2,3</sup>	1

Porosity (%)	1	20 <sup>4,5</sup> (10-30) <sup>4,5</sup>	1
--------------	---	--	---

<sup>1</sup>Mijnlieff (2020), <sup>2</sup>Mohammed (2020), <sup>3</sup>Doddema (2012), <sup>4</sup>Pijnenburg et al. (2019), <sup>5</sup>Lele et al. (2015)

### 1.1.5. Thermophysical properties

The **thermal conductivity** of halite crystals is ~5.5 W/m/K at 50°C. It varies between ~4.5 W/m/K at 100°C and ~6 W/m/K at 25°C (Urquhart and Bauer, 2015). Fuchs et al. (2015) even report 6.5 W/m/K for Halite. Daniilidis et al. (2016) use a wet heat conductivity of 3.5 W/m/K for the **Zechstein** salt in their model while Doddema (2012) use a value of 5.5 W/m/K. We assume a solid thermal conductivity of 4.5 W/m/K for the base case model with a possible variation between 3.5 and 6.5 W/m/K for the Zechstein salt layer. For the **Rotliegend** reservoir Daniilidis et al. (2016) use a wet thermal conductivity of 2.90 W/m/K. Doddema (2012) found values for sandstone mostly between ~2.5 W/m/K and ~3.5 W/m/K and used 3.0 W/m/K as wet heat conductivity of the Rotliegend reservoir layer. Considering a porosity of 20% and a thermal conductivity of 0.63 W/m/K (water at 20°C) one arrives at solid heat conductivities between ~3 W/m/K and 4.2 W/m/K. Blackwell and Steele (1989) provide thermal conductivity values of sandstones between 2.5 and 4.2 W/m/K. Fuchs et al. (2015) report thermal conductivity values of 7.7 W/m/K for quartz, 2-2.33 W/m/K for micas, and 1.9-2.25 W/m/K for feldspars. We assume a solid heat conductivity of the sandstone forming minerals for the Rotliegend reservoir of 3.5 W/m/K and a possible range from 3.0 W/m/K and 7.7 W/m/K. The **Limburg** layer is assumed to be a claystone in our model. Clays have thermal conductivity values between 1.8-1.85 W/m/K (Montmorillonite and Illite) and 2.7 W/m/K (Kaolinite) according to Fuchs et al. (2015). Daniilidis et al. (2016) use a wet heat conductivity of 2.65 W/m/K and Doddema (2012) uses 2.0 W/m/K for the Limburg group. While claystone thermal conductivities are ~2 W/m/K in the literature study of Doddema (2012), they also find higher values of 2.5 – 4 W/m/K for the Carboniferous. We assume a thermal conductivity of 2.0 W/m/K for the Limburg group in the base case scenario and assume a range between 1.8 W/m/K and 2.7 W/m/K (Table 5).

The **solid heat capacity** of halite crystals lies between 1920 J/m<sup>3</sup>/K (885 J/kg/K) and 2050 J/m<sup>3</sup>/K (945 J/kg/K) with no temperature dependence (Urquhart and Bauer, 2015). Waples and Waples (2004) report a solid heat capacity of 926 J/kg/K at 25°C. Daniilidis et al. (2016) and Doddema (2012) adopt a heat capacity of 1050 J/kg/K in their model of the **Zechstein** salt layer (combined heat capacity of solid and fluid). We use a solid heat capacity of 925 J/kg/K for the Zechstein layer in our base case model with a possible range between 885 and 950 J/kg/K. The heat capacity of quartz generally increases with temperature. Waples and Waples (2004) report a solid heat capacity of quartz of 740 J/kg/K at 20°C. Feldspars have heat capacities of 630-800 J/kg/K at 20°C (Waples and Waples, 2004) and plagioclase has a heat capacity between 711 and 837 J/kg/K at 20°C (Waples and Waples, 2004). For Quartzite and Microquartzite Waples and Waples (2004) report values of 1013 J/kg/K and 950 J/kg/K at 20°C. Daniilidis et al. (2016) use a heat capacity of 827 J/kg/K for their **Rotliegend** reservoir model and Doddema (2012) use 870 J/kg/K with a range of values determined from literature sources mainly between ~700 J/kg/K and ~1050 J/kg/K for sandstones. Given that our reservoir has an elevated temperature, we assume a base case solid heat capacity of the Rotliegend reservoir of 830 J/kg/°C with possible values between 650 and 1050 J/kg/°C. The heat capacity of clay is 860 J/kg/K at 20°C according to Waples and Waples (2004). Daniilidis et al. (2016) use a heat capacity of 840 J/kg/K for the Limburg formation and Doddema

(2012) used a value of 870 J/kg/K for the Carboniferous. We therefore assume a solid heat capacity of 860 J/kg/K with a range between 840 and 870 J/kg/K for the **Limburg** formation.

The **volumetric solid thermal expansion coefficient** is approximately three times the linear solid thermal expansion coefficient for isotropic rocks and minerals. We are using a volumetric thermal expansion in our model.

The undrained bulk thermal expansion coefficient can be expressed as:

$$\alpha_{bu} = \alpha_s + \Phi B(\alpha_f - \alpha_s),$$

with the solid (mineral) volumetric thermal expansion coefficient  $\alpha_s$ , the volumetric thermal expansion coefficient of the fluid  $\alpha_f$  and the Skempton coefficient B (McTigue, 1986). This would be representative of heating or cooling of rock with isolated (non-connected) pore space. In our model this is representative for the top seal (Zechstein) and the basement (Limburg). Since the porosity of these formations is negligible (1%) the effective bulk thermal expansion coefficient of the rock can be considered approximately equal to the solid volumetric thermal expansion coefficient.

The drained bulk thermal expansion coefficient of a fluid-saturated rock is equal to the bulk thermal expansion coefficient of dry rock (Jaeger et al., 2007). The drained bulk thermal expansion coefficient is representative for a porous and permeable geothermal sandstone reservoir, in our case the Rotliegend reservoir.

The drained volumetric bulk thermal expansion coefficient can be determined in the laboratory. The solid grain volumetric thermal expansion coefficients are also known.

The effect of the thermal expansion on the pore pressure is governed by the difference between the thermal expansion coefficients of pore fluid  $\alpha_f$  and pore volume  $\alpha_p$  (Zimmerman, 2010). This poro-elastic coupling effect is neglected in our simulations.

The volumetric thermal expansion coefficient of quartz is equal to 33.4e-6 1/°C (Palciauskas and Domenico, 1982). At higher temperatures this value slightly increases (37.2e-6 1/°C at 80°C based on Falzone and Stacey (1982)). The average thermal expansion coefficient of feldspars is 11.1e-6 1/°C (Fei, 1995), the solid thermal expansion coefficient of clay is 34e-6 1/°C (McTigue, 1986) and the solid thermal expansion coefficient of salt is between 120e-6 1/°C (McTigue, 1986) and 140e-6 1/°C (Skinner, 1966). For calcite, similar values are reported as for quartz (Srinivasan, 1955). Somerton (1992) report a linear thermal expansion coefficient of Quartz of 16 e-6 1/°C and linear thermal expansion coefficients of Berea, Bandera and Boise sandstone of 15-16e-6 1/°C under dry conditions and 13-20e-6 1/°C under saturated conditions. The drained bulk volumetric thermal expansion coefficient of Rothbach sandstone was measured as 28e-6 1/°C and calculated as 29.7e-6 1/°C by Ghabezloo and Sulem (2009). Hassanzadegan et al. (2012) determined a solid volumetric thermal expansion coefficient of a 10% porosity Flechtinger Sandstone to be 27.2e-6 1/°C. Plevová et al. (2011) determined thermal expansion coefficients of different Czech sandstones to be ~20e-6 1/°C. Zoback (2007) reports linear thermal expansion data from Griffith (1936). These values include ~10e-6 1/°C ( $\alpha_v \sim 30e-6$  1/°C) for Sandstones, ~11e-6 1/°C ( $\alpha_v \sim 33e-6$  1/°C) for Quartzites and Cherts, ~6.5e-6 1/°C ( $\alpha_v \sim 19.5e-6$  1/°C) for Andesites and ~8e-6 1/°C ( $\alpha_v \sim 24e-6$  1/°C) for Slates. Zoback (2007) states that the linear thermal expansion coefficient of silica is ~10e-6 1/°C ( $\alpha_v \sim 30e-6$  1/°C) while it is ~1e-6 1/°C ( $\alpha_v \sim 3e-6$  1/°C) for most other rock forming minerals. The Encyclopedia Britannica lists linear thermal expansion coefficients of rocks: sandstone 10+-2e-6 1/°C ( $\alpha_v \sim 30+-6e-6$  1/°C), limestone 8+-4e-6 1/°C ( $\alpha_v \sim 24+-12e-6$

1/°C), and slate  $9+1e-6$  1/°C ( $\alpha_v \sim 27+3e-6$  1/°C). Slizowski et al. (2015) determined volumetric thermal expansion coefficients of  $43-54e-6$  1/°C for polish Zechstein salt aggregates in laboratory experiments for the temperature range 20-100°C. The volumetric thermal expansion coefficient of anhydrite at room temperature was determined as  $36.6e-6$  1/°C by Evans (1979). Zhang et al. (2007) use a thermal expansion coefficient of Monfared et al. (2011) who determine the solid thermal expansion coefficient of Opalinus Claystone as  $30e-6$  1/°C. Since the experimental determination of the pore compressibility and pore thermal expansion coefficient is difficult, Monfared et al. (2011) assumed the pore compressibility and pore thermal expansion coefficient to be equal to the solid compressibility and solid thermal expansion coefficient.

Zhang et al. (2007) were modelling experiments on Opalinus Clay with bulk linear thermal expansion coefficients (they call it “wet”) of  $15e-6$  1/°C by using a fluid volumetric thermal expansion coefficient of  $340e-6$  1/°C and a solid linear thermal expansion coefficient of  $1.5e-6$  1/°C.

As indicated above, for the low porosity Zechstein and Limburg formations we assume that the bulk volumetric thermal expansion coefficient equals to the solid volumetric thermal expansion coefficient of the minerals, as also suggested by Palciauskas and Domenico (1982). The thermal expansion of liquid-saturated sandstones are not much different from dry sandstones (Somerton, 1992). Also, no large differences were found between the thermal expansion coefficients of Quartz and Sandstones. Therefore, we also assume that bulk thermal expansion coefficient is equal to solid thermal expansion coefficient for the Rotliegend formation.

For the base case scenario we use a **bulk volumetric thermal expansion coefficient** of  $30e-6$  1/°C for all three layers. Even though Halite has a volumetric thermal expansion coefficient of  $120e-6$  1/°C, the **Zechstein** is a very complex formation including additionally anhydrite ( $\alpha_v \sim 37e-6$  1/°C), carbonates ( $\alpha_v \sim 12-36e-6$  1/°C) and claystones ( $\alpha_v \sim 30e-6$  1/°C). Additionally, a much lower volumetric thermal expansion coefficient was determined for Zechstein rock samples in laboratory experiments ( $\alpha_v \sim 43-54e-6$  1/°C) and most other rock forming minerals have much lower thermal expansion coefficients in the order of  $3e-6$  1/°C. We therefore assume a bulk thermal expansion coefficient of  $30e-6$  1/°C for the **Rotliegend** reservoir in the base case scenario with a possible range between  $20e-6$  and  $35e-6$  1/°C. Additionally, specific thermal expansion scenarios will be considered in the sensitivity analysis. Since the solid thermal expansion coefficient of clay is similar to that of Quartz, we also use  $30e-6$  1/°C for the **Limburg** formation.

The **solid density** of halite is  $2.170$  kg/m<sup>3</sup>. Daniilidis et al. (2016) use the same value for the Zechstein formation in their model. We therefore use a solid density of  $2170$  kg/m<sup>3</sup> for the **Zechstein** layer. The actual solid density of the Zechstein layer may vary significantly (Doddema, 2012), but we do not consider this in our sensitivity analysis. Quartz has a solid density of  $2650$  kg/m<sup>3</sup> (Blake, 2008). This value is used for the **Rotliegend** reservoir layer in the base case model. Daniilidis et al. (2016) consider a density range of  $2500-2700$  kg/m<sup>3</sup>. We therefore adopt this range as approximate lower and upper bounds. The density of clay minerals typically ranges between  $2000$  and  $3000$  kg/m<sup>3</sup> while many are near  $2650$  kg/m<sup>3</sup> (Blake, 2008). We therefore use  $2650$  kg/m<sup>3</sup> as solid density of the **Limburg** layer in the base case scenario with a possible variation between  $2000$  and  $3000$  kg/m<sup>3</sup>.

*Table 5: Thermophysical properties of all model units. Values refer to rock matrix values unless otherwise stated.*

<b>Model property</b>	<b>Zechstein (rock salt)</b>	<b>Rotliegend (sandstone)</b>	<b>Limburg (claystone)</b>
Solid thermal conductivity (W/m/°C)	4.5 <sup>1</sup> (3.5 <sup>2</sup> -6.5 <sup>3</sup> )	3.5 (3.0 <sup>5</sup> -7.7 <sup>3</sup> )	2.0 <sup>5</sup> (1.8-2.7) <sup>3</sup>
Solid heat capacity (J/kg/°C)	925 <sup>4</sup> (885-950) <sup>1</sup>	830 <sup>2</sup> (650-1050)	860 <sup>4</sup> (840 <sup>2</sup> -870 <sup>5</sup> )
Volumetric bulk thermal expansion coefficient (1e-6/°C)	30 (30-55) <sup>12</sup>	30 <sup>9</sup> (20 <sup>11</sup> -40 <sup>8,10,14</sup> )	30 (15 <sup>13</sup> -50) <sup>7</sup>
Solid density (kg/m <sup>3</sup> )	2170 <sup>2</sup> (2100-2800) <sup>5</sup>	2650 <sup>5</sup> (2500-2700) <sup>2,5</sup>	2650 <sup>6</sup> (2000-3000) <sup>6</sup>

<sup>1</sup>Urquhart and Bauer (2015), <sup>2</sup>Daniilidis et al. (2016), <sup>3</sup>Fuchs et al. (2015), <sup>4</sup>Waples and Waples, 2004, <sup>5</sup>Doddema (2012), <sup>6</sup>Blake (2008), <sup>7</sup>McTigue, (1986), <sup>8</sup>Palciauskas and Domenico (1982), <sup>9</sup>Zoback (2007), <sup>10</sup>Falzone and Stacey (1982), <sup>11</sup>Plevová et al. (2011), <sup>12</sup>Slizowski et al. (2015), <sup>13</sup>Zhang et al.(2007), <sup>14</sup>Somerton (1992)

### 1.1.6. Fault properties

The fault is modelled as planar discontinuity with finite aperture. Fault asperities and roughness are not considered. In the base case scenario we assume that the fault has the same properties as the reservoir rock (100 mD permeability and 20% porosity). The fault **aperture**  $a$  is calculated from the **permeability**  $k$  using the cubic law:  $a = \sqrt{12k}$ . As upper and lower bound we assume 0 and 100% **porosity** and 0 and 10 D permeability (Table 6).

Hunfeld et al. (2017) determined fault friction coefficients of 0.66 for the Basal Zechstein, 0.37 for the Ten Boer claystone, 0.6 for the Rotliegend sandstone, and 0.5 for the Carboniferous. Even though other researchers (Buijze et al., 2017) use different fault friction coefficients for the different units as determined from these laboratory experiments (Hunfeld et al., 2017, 2020) and some fault cohesion between 0 and 3 MPa, we assume a cohesionless fault with a uniform **fault friction coefficient** of 0.6 that lies approximately between 0.5 and 0.7. This is mainly due to the inherent uncertainty in these parameters.

Most fault gauges tested by Hunfeld et al. (2017) showed velocity-strengthening behavior except for some cases of the Basal Zechstein anhydrite-carbonate material at the top of the Slochteren reservoir, which thus shows the highest seismogenic potential. However, as indicated above, we are using the same Rate-and-state friction (RSF) parameters for the entire fault.

*Table 6: Fault properties. Faults are represented as 2D planar surfaces without damage zone. Permeability is assumed to be independent of direction and faults are assumed to be filled to 100% with water. Thermophysical fault properties thus correspond to the properties of water. Permeability may vary from 0 (fault acts as hydraulic barrier) to above reservoir permeability values (fault acts as conduit).*

<b>Model property</b>	<b>Zechstein</b>	<b>Rotliegend</b>	<b>Limburg</b>
-----------------------	------------------	-------------------	----------------

	(rock salt)	(sandstone)	(claystone)
Fault friction coefficient (-)	0.6 (0.7) <sup>1,2</sup>	0.6 <sup>1,2</sup> (0.5-0.7) <sup>1</sup>	0.6 (0.5) <sup>1,2</sup>
Fault cohesion (MPa)	0	0	0
Fault aperture (m)	1.1e-6 (0-1.1e-5)	1.1e-6 (0-1.1e-5)	1.1e-6 (0-1.1e-5)
Fault permeability (mD)	100 (0-10000)	100 (0-10000)	100 (0-10000)
Fault porosity (%)	20 (0-100)	20 (0-100)	20 (0-100)
RSF a-value (-)	0.005 <sup>1</sup> (0.001 – 0.03) <sup>1</sup>	0.005 <sup>1</sup> (0.001 – 0.03) <sup>1</sup>	0.005 <sup>1</sup> (0.001 – 0.03) <sup>1</sup>
RSF b-value (-)	0.0025 <sup>1</sup> (-0.006 – 0.03) <sup>1</sup>	0.0025 <sup>1</sup> (-0.006 – 0.03) <sup>1</sup>	0.0025 <sup>1</sup> (-0.006 – 0.03) <sup>1</sup>
RSF (a-b)-value (-)	0.0025 <sup>1</sup> (-0.003 – 0.012) <sup>1</sup>	0.0025 <sup>1</sup> (-0.003 – 0.012) <sup>1</sup>	0.0025 <sup>1</sup> (-0.003 – 0.012) <sup>1</sup>
RSF critical slip distance d <sub>c</sub> (mm)	1e-5 <sup>1</sup> (2e-6 – 3e-4) <sup>1</sup>	1e-5 <sup>1</sup> (2e-6 – 3e-4) <sup>1</sup>	1e-5 <sup>1</sup> (2e-6 – 3e-4) <sup>1</sup>

<sup>1</sup>Hunfeld et al. (2017, 2020), <sup>2</sup>Buijze et al. (2017)

### 1.1.7. Reservoir fluid data

The reservoir fluid is saline water (brine) with **pressure and temperature dependent fluid properties**. For the base case model we use fluid density, viscosity, heat capacity and bulk modulus determined for the Groß Schönebeck (GrSk) site (NaCl, KCl, and CaCl<sub>2</sub> molality of 1.815, 0.043 and 1.399, respectively) using the code BrineProp\_0.7.3.1 (Francke et al., 2013). A 5 mol NaCl/kg H<sub>2</sub>O solution, which has a similar salinity as the Groß Schönebeck fluid, was assumed for the volumetric thermal expansion coefficient and the thermal conductivity. From Table 7 it is obvious that the viscosity and thermal expansion coefficient have the largest temperature/pressure dependence. Additionally, taking into account the salinity is important for all parameters. For viscosity a temperature and pressure dependent look-up table is used. Bulk modulus, thermal conductivity, density and heat capacity are almost not affected by pressure and temperature changes. Thus, constant values are assumed here. Even though the fluid thermal expansion coefficients are provided in Table 7, we do not explicitly implement them in the model as fluid thermal expansion is integrated into the pore thermal expansion coefficient provided in Table 5.

The fluid thermal expansion and hence the fluid mass change is considered by the temperature dependence of the fluid density. The fluid thermal expansion coefficient is not explicitly used in the model.

For the sensitivity analysis we use the pressure and temperature dependent water properties from REFPROP (Lemmon et al., 2018) and typical variations within the expected salinity range of 0-400 g/l and pressure and temperature range.

Table 7: Pure water properties and hypothetical reservoir fluid based on the Groß Schönebeck Rotliegend water properties for pressure and temperature conditions found at injection well (30°C and 30 MPa) and production well (80°C and 20 MPa). Additionally, the properties for the base case model and sensitivity analysis are summarized.

Model property	H2O at 30°C and 30 MPa	H2O at 80°C and 20 MPa	GrSk fluid at 30°C and 30 MPa	GrSk fluid at 80°C and 20 MPa	Base case model	Sensitivity
Density (kg/m <sup>3</sup> )	1009 <sup>1</sup>	980 <sup>1</sup>	1185 <sup>2</sup>	1154 <sup>2</sup>	f(P/T) <sub>GrSk</sub>	f(P/T) <sub>H2O</sub> , 980, 1200
Viscosity (mPas)	0.80 <sup>1</sup>	0.36 <sup>1</sup>	1.51 <sup>2</sup>	0.68 <sup>2</sup>	f(P/T) <sub>GrSk</sub>	f(P/T) <sub>H2O</sub> , 0.3, 1.5
Volumetric thermal expansion coefficient (1/°C)	3.27e-4 <sup>1</sup>	6.21e-4 <sup>1</sup>	4.10e-4 <sup>3,*</sup>	5.40e-4 <sup>3,*</sup>	-	-
Specific heat capacity (J/kg/°C)	4106 <sup>1</sup>	4156 <sup>1</sup>	3227 <sup>2</sup>	3248 <sup>2</sup>	3240	3200 - 4200
Thermal conductivity (W/m/°C)	0.629 <sup>1</sup>	0.680 <sup>1</sup>	0.595 <sup>4,*</sup>	0.649 <sup>4,*</sup>	0.625	0.6 – 0.7
Bulk modulus (GPa)	2.41 <sup>1</sup>	2.30 <sup>1</sup>	3.70 <sup>2</sup>	3.41 <sup>2</sup>	3.4	2.0 – 4.0

<sup>1</sup>Lemmon et al. (2018), <sup>2</sup>Francke et al. (2013), <sup>3</sup>Rogers and Pitzer (1982), <sup>4</sup>Aleksandrov et al. (2013), \*value for 5mol NaCl solution, GrSk=Groß Schönebeck

### 1.1.8. Operational and wellbore data

According to Mijnlief (2020) the **flow rate** of geothermal wells accessing the Slochteren reservoir ranges from ~30 to ~100 l/s. We chose these values as limits and a flow rate of 70 l/s as representative for the base case scenario.

The **well spacing** (distance between production and injection well) is typically far enough to avoid thermal breakthrough of the cold injection water at the production well. The well spacing of Dutch geothermal doublets is up to 1.5 km (Mijnlief, 2020). We therefore use 1.5 km as maximum well spacing. For the base case, we use a typical well spacing of 1 km and 0.5 km represents our lower bound for the sensitivity analysis.

Even though most of the Dutch geothermal wells are inclined, we use vertical wells for the base case scenario.

Typically, a **re-injection temperature** of 25-35°C is assumed for (Dutch) geothermal wells (Hurter and Schellschmidt, 2003; Wang et al., 2019; Willems et al., 2017). Therefore, we use a re-injection temperature of 30°C for the base case scenario. To evaluate the effect of a further reduction of re-injection temperature we use 15°C as the lower bound, which is 15°C below the base case. An upper bound of 45°C is used, which is 15°C above the base case.

We do not model the entire geothermal wellbores explicitly but approximate them as open 1D elements going through the entire reservoir layer. Therefore, we do not consider the wellbore diameter in our sensitivity analysis. However, we use a typical geothermal **wellbore diameter** of 8 1/2" for the open hole section in all models.

Finding a safe distance between geothermal well doublets and a critically stressed fault is a major critical question. We use a **distance between wells and fault** of 250 m for the base case scenario in order to easily see effects of different parameters on the temperature, pressure and stress distribution on the fault. For the sensitivity analysis we vary this distance between 0 m (well intersects the fault) and 1000 m (Table 8).

*Table 8: Operational and wellbore data. Operations are typically year-round (up to 8670 hr/a; Mijnlief, 2020).*

<b>Model property</b>	<b>Value</b>
Distance between wells and fault (m)	250 (0-1000)
Well spacing (m)	1000 (500-1500 <sup>1</sup> )
Well inclination from vertical (°)	0
Re-injection temperature (°C)	30 <sup>2,3,4</sup> (15-45)
Flow rate (l/s)   Flow rate (m <sup>3</sup> /hr)	70 (30 <sup>1</sup> -100 <sup>1</sup> )   ~250 (~110 <sup>1</sup> -~350 <sup>1</sup> )
Length of perforated/open interval (m)	Throughout the reservoir unit
Wellbore diameter (inch)	8 1/2

<sup>1</sup>Mijnlief (2020), <sup>2</sup>Hurter and Schellschmidt, 2003, <sup>3</sup>Wang et al., 2019, <sup>4</sup>Willems et al., 2017

## 1.2. Modeling scenarios

First, the base case model is simulated. Then, a sensitivity analysis of the most important geometries, reservoir parameters and operational parameters is performed (Table 9). Based on the sensitivity analysis several specific scenarios were derived (Table 10). The base case model is setup using the parameters provided in the previous section. The sensitivity analysis is performed within the parameter range given in the brackets.

To investigate the effect of Seismogenic Index on the Coulomb failure stress model results, we

also changed this value for the Slochteren base case scenario between -6 and -3 (S1a,b), while the base case value was -4.5 in all scenarios.

Table 9: Summary of modeling scenarios for the sensitivity analysis (RI).

Scenario ID	Changed parameter	Changed values
S1	Base case scenario	-
S1a,b	Seismogenic index	-6, -3
<b>Geometry of reservoir, top and bottom seal, and faults</b>		
S2a,b	Depth of reservoir top	1500 m, 3000 m
S3a,b	Reservoir thickness	100 m, 250 m
S4	Fault strike	N150°E
S5a,b,c	Fault dip	60°, 70°, 85°
<b>Geomechanical reservoir properties</b>		
S6a,b	Young's modulus reservoir	3 GPa, 30 GPa
S7a,b	Poisson's ratio reservoir	0.10, 0.25
S8a,b	Biot coefficient reservoir	0.5, 0.97
<b>Hydraulic reservoir properties</b>		
S9a,b	Hor. permeability	50 mD, 350 mD
S10a,b	Hor./vert. permeability	1, 10
S11a,b	Porosity	10%, 30%
<b>Thermophysical reservoir properties</b>		
S12a,b	Thermal conductivity reservoir rock	3.0 W/m/°C, 7.7 W/m/°C
S13a,b	Heat capacity reservoir rock	650 J/kg/°C, 1050 J/kg/°C
S14a,b	Thermal expansion coefficient (solid+fluid)	20e-6 1/°C, 40e-6 1/°C
<b>Fault properties</b>		
S15a,b	Fault permeability, porosity	0 D & 0%, 10 D & 100%
<b>Temperature, pressure, stress</b>		
S16a,b	Temperature gradient	20°C/km + 10°C, 40°C/km + 10°C
S17a,b	Pressure gradient	10 MPa/km, 12 MPa/km
S18a,b	Vertical stress gradient	21/15/14 MPa/km, 23/15/14 MPa/km
S19a,b	Maximum horizontal stress gradient	22/14/14 MPa/km, 22/20/14 MPa/km
S20a,b	Minimum horizontal stress gradient	22/15/13 MPa/km, 22/20/20 MPa/km
S21a,b,c,d	Maximum horizontal stress direction	N150°E, N170°E
<b>Fluid properties</b>		
S22a,b	Density	980 kg/m <sup>3</sup> , 1200 kg/m <sup>3</sup>
S23a,b	Viscosity	0.3 mPas, 1.5 mPas
S24a,b	Specific heat capacity	3200 J/kg/°C, 4200 J/kg/°C
S25a,b	Thermal conductivity	0.6 W/m/K, 0.7 W/m/K
S26a,b	Bulk modulus	2 GPa, 4 GPa
<b>Operational and wellbore data</b>		

S27a,b	Well spacing	500 m, 1500 m
S28a,b,c	Re-injection temperature	15°C, 45°C
S29a,b,c	Flow rate	30 l/s, 100 l/s
S30a,b,c	Well position	Wells intersect fault; injection well 500 m, 1000 m from fault
<b>Processes</b>		
S32	Thermoelastic effects	Thermal expansion coefficient = 0

S33: The low transmissivity scenario describes a scenario where the hydraulic and mechanical parameters represent a low porosity and permeability reservoir. According to Mijnlief (2020) the minimum transmissivity is 10 Dm for economic geothermal production. We therefore use this as lower limit.

S34: The high transmissivity scenario describes a scenario where the hydraulic and mechanical parameters represent a high porosity and permeability reservoir. According to Mijnlief (2020) the maximum transmissivity in the Dutch Rotliegend formation is 50 Dm. We therefore use this upper limit.

S35: The influence of the fault offset is analysed by a simulation of the base case scenario with a 100 m vertical downward displacement of the hanging wall.

*Table 10: Summary of specific modeling scenarios for the Slochteren sandstone reservoir.*

<b>Scenario ID</b>	<b>Description</b>	<b>Changed values</b>
S33	Deep low porosity reservoir	D=3000 m, H=100 m, k=100 mD, T=10 Dm, $k_h/k_v=10$ , $\phi=10\%$ , $\alpha=0.5$ , E=30 GPa, $\nu=0.1$ , q=40 l/s
S34	Shallow high porosity reservoir	D=1500 m, H=250 m, k=200 mD, T=50 Dm, $k_h/k_v=1$ , $\phi=30\%$ , $\alpha=0.97$ , E=3 GPa, $\nu=0.25$ , q=100 l/s
S35	Fault offset (Figure 2)	Fault offset=100 m

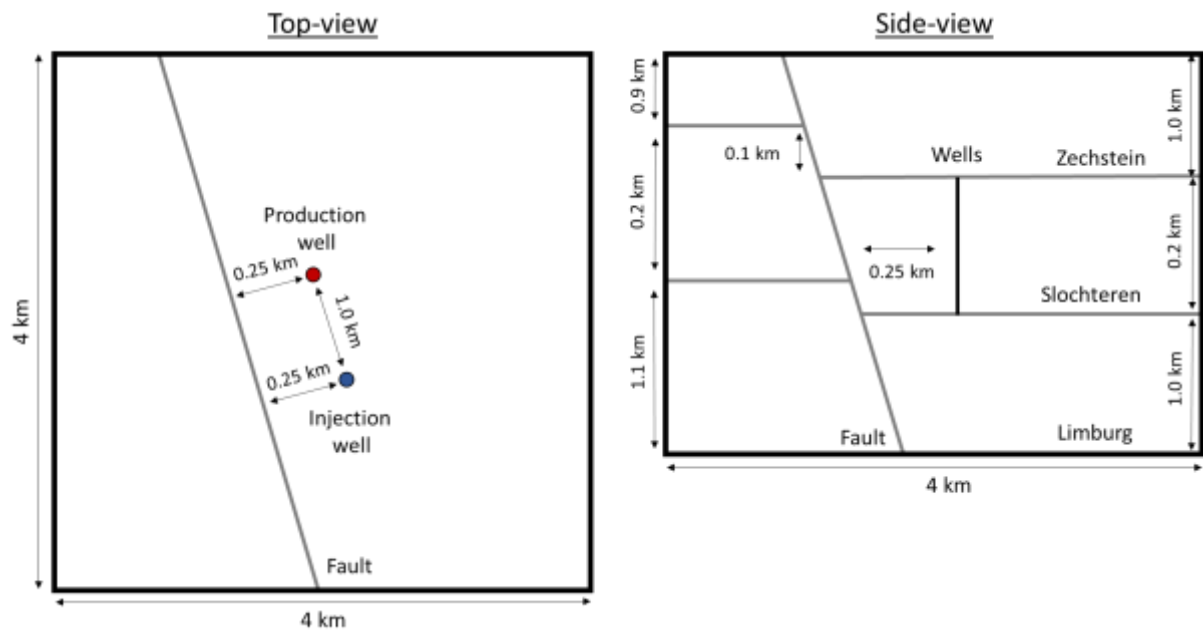


Figure 2: Sketch of the Slochteren model with fault offset (Scenario S35; not to scale).

## 2. Delft Sandstone

This section describes the hydrothermal reservoir properties above the Permian salt in the Netherlands. The considered reservoir formation is the Delft Sandstone Member. This massive sandstone sequence is overlain by the Rodenrijs Member, an organic rich claystone, which is used as the top layer in this model. The Alblasserdam Member (flood-plain deposits) is used as the bottom layer in this model.

Conceptually, we thus simplify the geology to a conceptual model consisting of a horizontal claystone layer (Rodenrijs Member) as top seal, a horizontal high net to gross sandstone layer (Delft Sandstone) as reservoir unit and a horizontal low net to gross sandstone/claystone layer (Alblasserdam Member) as basement. All layers are intersected by a single inclined fault (Figure 3). No fault offset is assumed. Hot water production and cold-water injection is modelled through a typical Dutch geothermal well doublet. Both wells are vertical and intersect the entire Delft sandstone reservoir. They are assumed to be open to flow along the entire well path inside the reservoir formation.

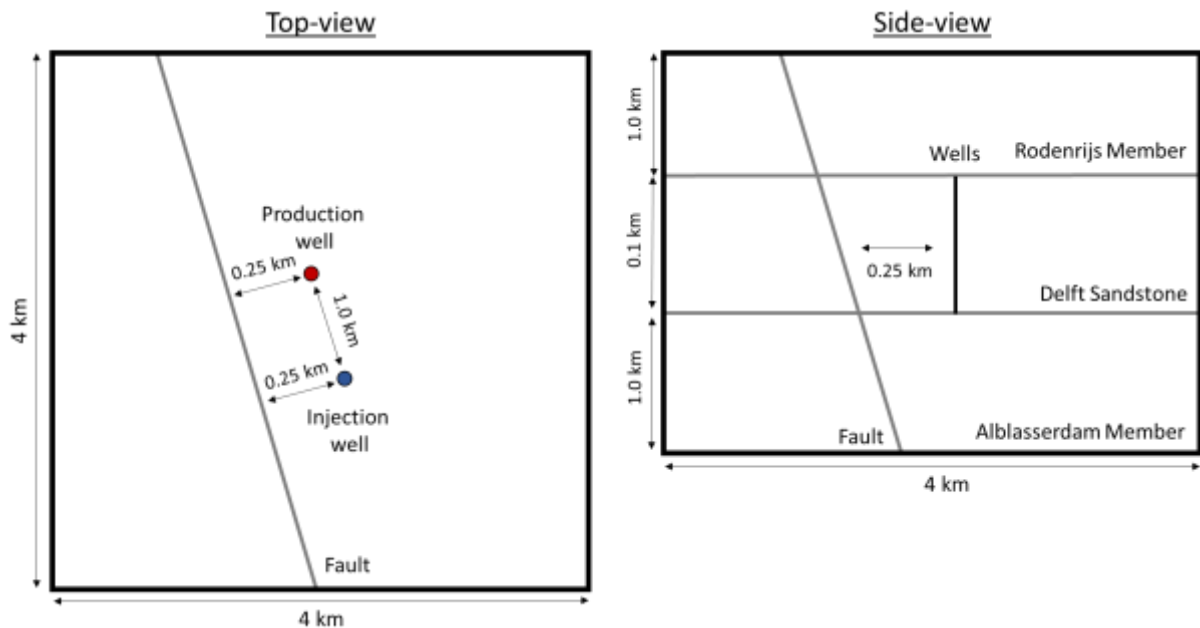


Figure 3: Conceptual numerical model setup for the Delft sandstone reservoir (not to scale).

### 2.1. Data summary

#### 2.1.1. Geological model geometry

The same geometry is used as for the Slochteren model. The top layer was artificially extended to 1000 m to avoid boundary effects in the model, thus integrating all overlaying formations as well. The thickness of the Alblasserdam Member varies significantly between <100 m and >1300 m. A thickness of 1000 m is chosen as representative for the bottom layer. The same fault is used as in the Slochteren model (Table 11).

Table 11: Model geometry data. For the numerical model the faults are assumed to intersect all

three layers and extend laterally through the entire model since fault lengths are estimated to be >10 km based on de Jager (2007). A typical fault spacing of ~5 km (de Jager, 2007) warrants using a single fault only in the models.

Model property	Rodenrijs Member (claystone)	Delft Sandstone Member	Alblasserdam Member (sst/clst)
Unit top (m)	1300	2300 (1850-2500)	2400
Unit thickness (m)	1000 (10-130)	100 (60-140)	1000 <sup>2</sup> (<100 - >1300) <sup>2</sup>
Fault strike	N130°E <sup>1,3</sup> (N150°E <sup>1,3</sup> )	N130°E <sup>1,3</sup> (N150°E <sup>1,3</sup> )	N130°E <sup>1,3</sup> (N150°E <sup>1,3</sup> )
Fault dip (° from horizontal)	80 <sup>3</sup> (60-85) <sup>3</sup>	80 <sup>3</sup> (60-85) <sup>3</sup>	80 <sup>3</sup> (60-85) <sup>3</sup>
Fault dip direction	NE <sup>3</sup>	NE <sup>3</sup>	NE <sup>3</sup>

<sup>1</sup>Duin et al. (2006), <sup>2</sup>TNO-GSN (2021c), <sup>3</sup>de Jager (2007)

### 2.1.2. Stress, pressure and temperature data

The same temperature, pressure and stress gradients as well as heat flow values are used as in the Slochteren Model (Table 12).

Table 12: Stress, pressure and temperature data. Note that both horizontal stress gradients equal to the vertical stress gradient in the Zechstein layer.

Model property	Value
Heat flow	70 mW/m <sup>2</sup> <sup>1</sup>
Temperature gradient	31°C/km (20-40°C/km) + 10°C <sup>1</sup>
Pore pressure gradient	11 MPa/km (10-12 MPa/km) <sup>2</sup>
Vertical stress gradient	22 MPa/km (21-23 MPa/km) <sup>3</sup>
Maximum horizontal stress gradient	15 MPa/km (14-20 MPa/km) <sup>4</sup>
Minimum horizontal stress gradient	14 MPa/km (13-20 MPa/km) <sup>3</sup>
Maximum horizontal stress direction	N160°E (N150°E-N170°E) <sup>5</sup>

<sup>1</sup>Bonté et al. (2012), <sup>2</sup>Verweij et al., 2012, <sup>3</sup>TNO (2015), <sup>4</sup>van Eijs (2015), <sup>5</sup>Heidbach et al. (2016) and Mechelse (2017)

### 2.1.3. Geomechanical properties

No consistent literature values were found for Rodenrijs, Delft Sandstone and Alblasterdam. Therefore, the values from the Slochteren model were used for Sandstone and Claystone. For the Alblasterdam Member approximately average values between Rodenrijs Member and Delft Sandstone Member were used (Table 13).

Table 13: Elastic properties of all model units.

Model property	Rodenrijs Member (claystone)	Delft Sandstone Member	Alblasterdam Member (sst/clst)
Young's modulus (GPa)	40 <sup>1</sup>	15 (3-30) <sup>1,2</sup>	25
Poisson's ratio (-)	0.2 <sup>1</sup>	0.2 <sup>1,2</sup> (0.1-0.25) <sup>1,2</sup>	0.2
Solid bulk modulus (GPa)	50 <sup>5</sup>	40 <sup>3</sup>	45
Drained bulk modulus* (GPa)	22.2	8.33 (1.3-20)	13.9
Biot coefficient* (-)	0.56	0.86 <sup>1,4</sup> (0.5-0.97) <sup>1,4</sup>	0.69

<sup>1</sup>Lele et al. (2015), <sup>2</sup>Pijnenburg et al. (2019), <sup>3</sup>Schmitt (2015), <sup>4</sup>Trautwein (2005), <sup>5</sup>Delage (2013), \*calculated

#### 2.1.4. Hydraulic properties

Compared to the Slochteren reservoir, the Delft Sandstone Member has a higher permeability. The top and bottom layers have a higher porosity (Table 14).

Table 14: Hydraulic properties of all model units.

Model property	Rodenrijs Member (claystone)	Delft Sandstone Member	Alblasterdam Member (sst/clst)
Hor. permeability (mD)	1	1000 <sup>1</sup> (>10-3000) <sup>1</sup>	1
Hor./vert. permeability (-)	1	2 (1-10) <sup>2,3</sup>	1
Porosity (%)	10	20 <sup>1</sup> (10-25) <sup>1</sup>	10

<sup>1</sup>Willems et al. (2020), <sup>2</sup>Mohammed (2020), <sup>3</sup>Doddema (2012)

#### 2.1.5. Thermophysical properties

Thermophysical properties (Table 15) of the Delft Sandstone layer were based on the Slochteren Sandstone model and adapted based on Willems et al. (2020). Rodenrijs properties were based on the claystone properties from the Slochteren model and Alblasterdam properties were based on a mix between sandstone and claystone properties with specific information taken from Willems et

al. (2020).

Table 15: Thermophysical properties of all model units. Values refer to rock matrix values unless otherwise stated.

Model property	Rodenrijs Member (claystone)	Delft Sandstone Member	Alblasserdam Member (sst/clst)
Solid thermal conductivity (W/m/°C)	2.0 <sup>4</sup>	4.5 <sup>1</sup> (3.0 <sup>4</sup> -7.7 <sup>2</sup> )	2.5 <sup>12</sup>
Solid heat capacity (J/kg/°C)	950 <sup>12</sup>	730 <sup>15</sup> (650-1050)	860 <sup>3</sup>
Volumetric bulk thermal expansion coefficient (1e-6/°C)	30 (15 <sup>9</sup> -50) <sup>6</sup>	30 <sup>9</sup> (20 <sup>11</sup> -40 <sup>7,8,10</sup> )	30 (15 <sup>9</sup> -50) <sup>6</sup>
Solid density (kg/m <sup>3</sup> )	2650 <sup>5,12</sup>	2650 <sup>12</sup>	2650 <sup>5,12</sup>

<sup>1</sup>Urquhart and Bauer (2015), <sup>2</sup>Fuchs et al. (2015), <sup>3</sup>Waples and Waples, 2004, <sup>4</sup>Doddema (2012), <sup>5</sup>Blake (2008), <sup>6</sup>McTigue, (1986), <sup>7</sup>Palciauskas and Domenico (1982), <sup>8</sup>Falzone and Stacey (1982), <sup>9</sup>Zhang et al.(2007), <sup>10</sup>Somerton (1992), <sup>11</sup>Plevová et al. (2011), <sup>12</sup>Willems et al. (2020)

### 2.1.6. Fault properties

For the Delft Sandstone model, the same fault properties as in the Slochteren Sandstone model were used (Table 16).

Table 16: Fault properties. Faults are represented as 2D surfaces without damage zone. Permeability is assumed to be independent of direction and faults are assumed to be filled to 100% with water. Thermophysical fault properties thus correspond to the properties of water. Permeability may vary from 0 (fault acts as hydraulic barrier) to above reservoir permeability values (fault acts as conduit).

Model property	Rodenrijs Member (claystone)	Delft Sandstone Member	Alblasserdam Member (sst/clst)
Fault friction coefficient (-)	0.6 (0.7) <sup>1,2</sup>	0.6 <sup>1,2</sup> (0.5-0.7) <sup>1</sup>	0.6 (0.5) <sup>1,2</sup>
Fault cohesion (MPa)	0	0	0
Fault aperture (m)	1.1e-6 (0-1.1e-5)	3.44e-6 (0-1.1e-5)	1.1e-6 (0-1.1e-5)
Fault permeability (mD)	100 (0-10000)	1000 (0-10000)	100 (0-10000)
Fault porosity (%)	20 (0-100)	20 (0-100)	20 (0-100)

RSF a-value (-)	0.005 <sup>1</sup> (0.001 – 0.03) <sup>1</sup>	0.005 <sup>1</sup> (0.001 – 0.03) <sup>1</sup>	0.005 <sup>1</sup> (0.001 – 0.03) <sup>1</sup>
RSF b-value (-)	0.0025 <sup>1</sup> (-0.006 – 0.03) <sup>1</sup>	0.0025 <sup>1</sup> (-0.006 – 0.03) <sup>1</sup>	0.0025 <sup>1</sup> (-0.006 – 0.03) <sup>1</sup>
RSF (a-b)-value (-)	0.0025 <sup>1</sup> (-0.003 – 0.012) <sup>1</sup>	0.0025 <sup>1</sup> (-0.003 – 0.012) <sup>1</sup>	0.0025 <sup>1</sup> (-0.003 – 0.012) <sup>1</sup>
RSF critical slip distance d <sub>c</sub> (mm)	1e-5 <sup>1</sup> (2e-6 – 3e-4) <sup>1</sup>	1e-5 <sup>1</sup> (2e-6 – 3e-4) <sup>1</sup>	1e-5 <sup>1</sup> (2e-6 – 3e-4) <sup>1</sup>

<sup>1</sup>Hunfeld et al. (2017, 2020), <sup>2</sup>Buijze et al. (2017)

### 2.1.7. Reservoir fluid data

Due to the lack of reservoir fluid data, we assume pure water as representative reservoir fluid for the Delft Sandstone model (Table 17).

*Table 17: Pure water properties and hypothetical reservoir fluid based on the Groß Schönebeck Rotliegend water properties for pressure and temperature conditions found at injection well (30°C and 30 MPa) and production well (80°C and 20 MPa). Additionally, the properties for the base case model and sensitivity analysis are summarized.*

Model property	H2O at 30°C and 30 MPa	H2O at 80°C and 20 MPa	GrSk fluid at 30°C and 30 MPa	GrSk fluid at 80°C and 20 MPa	Base case model	Sensitivity
Density (kg/m <sup>3</sup> )	1009 <sup>1</sup>	980 <sup>1</sup>	1185 <sup>2</sup>	1154 <sup>2</sup>	f(P/T) <sub>H2O</sub>	-
Viscosity (mPas)	0.80 <sup>1</sup>	0.36 <sup>1</sup>	1.51 <sup>2</sup>	0.68 <sup>2</sup>	f(P/T) <sub>H2O</sub>	-
Volumetric thermal expansion coefficient (1/°C)	3.27e-4 <sup>1</sup>	6.21e-4 <sup>1</sup>	4.10e-4 <sup>3,*</sup>	5.40e-4 <sup>3,*</sup>	-	-
Specific heat capacity (J/kg/°C)	4106 <sup>1</sup>	4156 <sup>1</sup>	3227 <sup>2</sup>	3248 <sup>2</sup>	4125	-
Thermal conductivity (W/m/°C)	0.629 <sup>1</sup>	0.680 <sup>1</sup>	0.595 <sup>4,*</sup>	0.649 <sup>4,*</sup>	0.65	-

Bulk modulus (GPa)	2.41 <sup>1</sup>	2.30 <sup>1</sup>	3.70 <sup>2</sup>	3.41 <sup>2</sup>	2.35	-
--------------------	-------------------	-------------------	-------------------	-------------------	------	---

<sup>1</sup>Lemmon et al. (2018), <sup>2</sup>Francke et al. (2013), <sup>3</sup>Rogers and Pitzer (1982), <sup>4</sup>Aleksandrov et al. (2013), \*value for 5mol NaCl solution, GrSk=Groß Schönebeck

### 2.1.8. Operational and wellbore data

The same operational and wellbore data were used in the Delft Sandstone model as in the Slochteren Sandstone model (Table 18).

Table 18: Operational and wellbore data. Operations are typically year-round (up to 8670 hr/a; Mijnlief, 2020).

Model property	Value
Distance between wells and fault (m)	250 (0-1000)
Well spacing (m)	1500 (1000-2000 <sup>1</sup> )
Well inclination from vertical (°)	0
Re-injection temperature (°C)	30 <sup>2,3,4</sup> (15-45)
Flow rate (l/s)   Flow rate (m <sup>3</sup> /hr)	70 (30 <sup>1</sup> -100 <sup>1</sup> )   ~250 (~110 <sup>1</sup> ~350 <sup>1</sup> )
Length of perforated/open interval (m)	Throughout the reservoir unit
Wellbore diameter (inch)	8 1/2

<sup>1</sup>Mijnlief (2020), <sup>2</sup>Hurter and Schellschmidt, 2003, <sup>3</sup>Wang et al., 2019, <sup>4</sup>Willems et al., 2017

### 2.2. Modelling scenarios

Besides the base case Delft Sandstone model, a small sensitivity analysis is performed for the re-injection temperature (Table 19).

Table 19: Summary of specific modelling scenarios for the Delft sandstone member.

Scenario ID	Description	Changed values
S36	Delft base case	-
S37a,b	Re-injection temperature	T=15°C, T=45°C

### 3. Dinantian limestone

The Dinantian carbonate formation is the deepest formation we consider in our analysis. Here, we simplify the geology to a horizontal Limburg claystone layer as top seal, a horizontal Dinantian limestone layer as reservoir layer and a horizontal Devonian claystone-sandstone layer as bottom seal. Due to the low permeability of the rock matrix we consider two models for geothermal exploitation of the Dinantian limestone: a) wells intersect a high permeability fault (“Dinantian fault model”; Figure 4), b) wells intersect a fault zone (“Dinantian fault damage zone model”; Figure 5), and c) hydraulically fractured parallel horizontal wells are drilled next to the fault representing a multi-stage Enhanced Geothermal System (“Dinantian EGS model”; Figure 6).

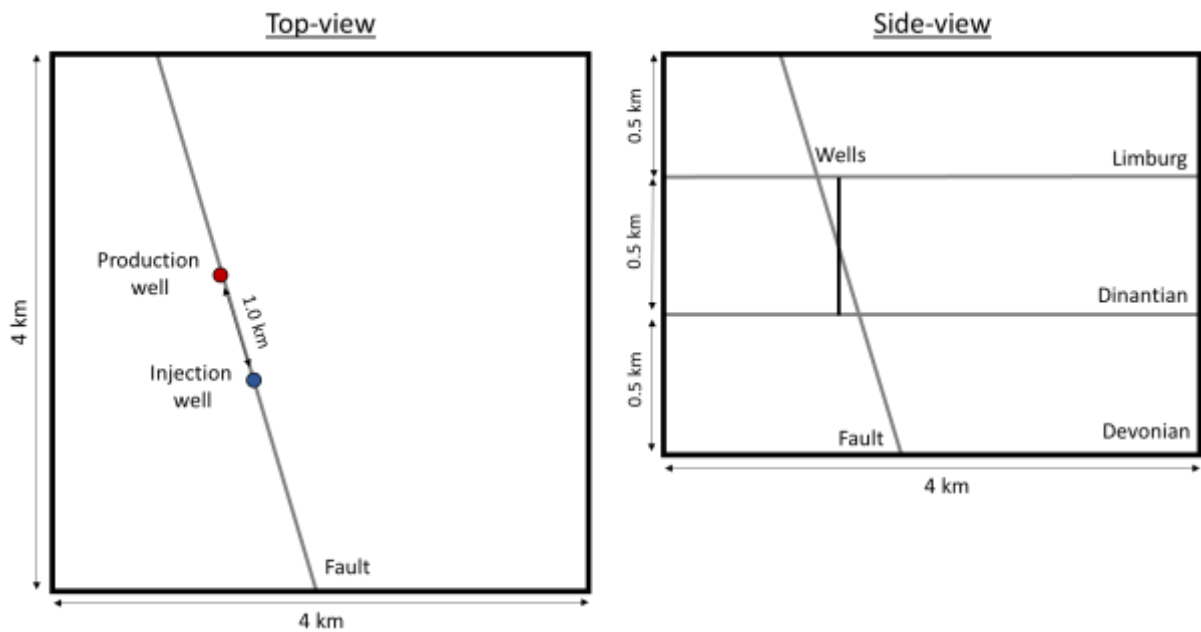


Figure 4: Conceptual sketch of the Dinantian fault model (not to scale).

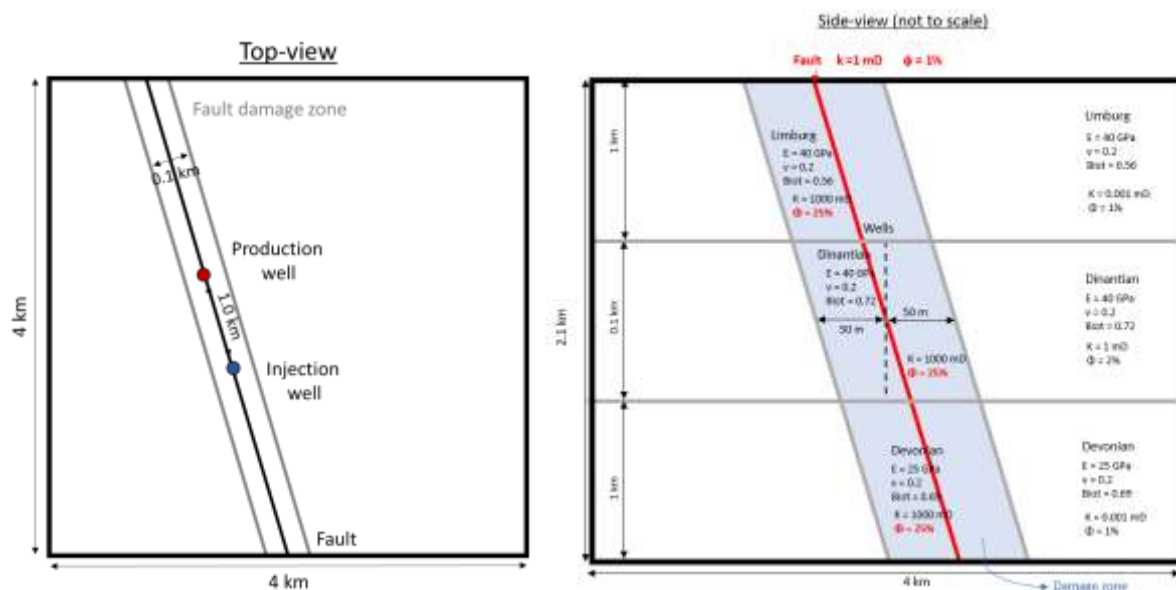


Figure 5: Conceptual sketch of the Dinantian fault damage zone model (not to scale).

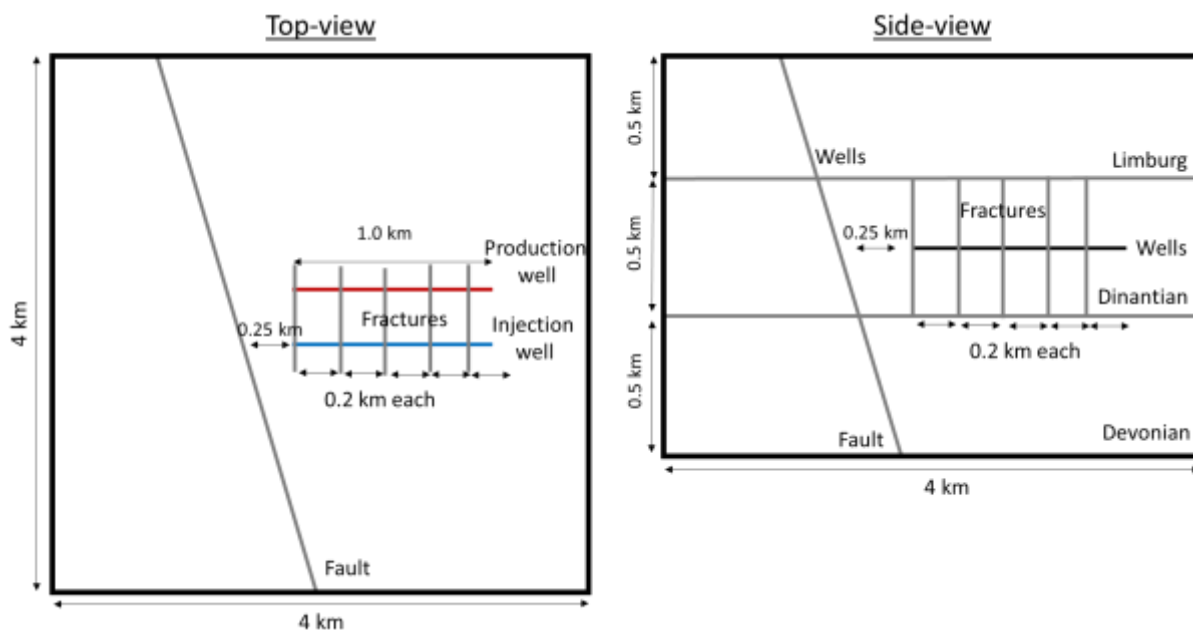


Figure 6: Conceptual sketch of the Dinantian EGS model (not to scale).

### 3.1. Data summary

#### 3.1.1. Geological model geometry

The depth of the Dinantian varies between 2 and 9 km. For the considered Ultra Deep Geothermal development with temperatures  $>120^{\circ}\text{C}$  we use a 4.5 km deep Dinantian reservoir top. A thickness of 500 m is assumed. The same thickness is used for the top and bottom layers. Fault geometry and properties are the same as in the Slochteren model (Table 20).

Table 20: Model geometry data. For the numerical model the faults are assumed to intersect all three layers and extend laterally through the entire model since fault lengths are estimated to

be >10 km based on de Jager (2007). A typical fault spacing of ~5 km (de Jager, 2007) warrants using a single fault only in the models.

Model property	Limburg (claystone)	Dinantian (limestone)	Devonian (clst/sst)
Unit top (m)	4000	4500 (2000-9000)	5000
Unit thickness (m)	500 (<900)	500 (<750)	500 (<300)
Fault strike	N130°E <sup>1,2</sup> (N150°E <sup>1,2</sup> )	N130°E <sup>1,2</sup> (N150°E <sup>1,2</sup> )	N130°E <sup>1,2</sup> (N150°E <sup>1,2</sup> )
Fault dip (° from horizontal)	80 <sup>2</sup> (60-85) <sup>2</sup>	80 <sup>2</sup> (60-85) <sup>2</sup>	80 <sup>2</sup> (60-85) <sup>2</sup>
Fault dip direction	NE <sup>2</sup>	NE <sup>2</sup>	NE <sup>2</sup>

<sup>1</sup>Duin et al. (2006), <sup>2</sup>de Jager (2007)

### 3.1.2. Stress, pressure and temperature data

All stress, pressure and temperature initial and boundary conditions are the same as in the Slochteren model adapted for the depth (Table 21).

Table 21: Stress, pressure and temperature data.

Model property	Value
Heat flow	70 mW/m <sup>2</sup> <sup>1</sup>
Temperature gradient	31°C/km (20-40°C/km) + 10°C <sup>1</sup>
Pore pressure gradient	11 MPa/km (10-12 MPa/km) <sup>2</sup>
Vertical stress gradient	22 MPa/km (21-23 MPa/km) <sup>3</sup>
Maximum horizontal stress gradient	15 MPa/km (14-20 MPa/km) <sup>4</sup>
Minimum horizontal stress gradient	14 MPa/km (13-20 MPa/km) <sup>3</sup>
Maximum horizontal stress direction	N160°E (N150°E-N170°E) <sup>5</sup>

<sup>1</sup>Bonté et al. (2012), <sup>2</sup>Verweij et al., 2012, <sup>3</sup>TNO (2015), <sup>4</sup>van Eijs (2015), <sup>5</sup>Heidbach et al. (2016) and Mechelse (2017)

### 3.1.3. Geomechanical properties

The description of the Limburg properties can be found in the respective sections on the Slochteren model. The Devonian properties are an approximate average of claystone and sandstone and thus

correspond to the Alblasserdam Member as defined above. For the Dinantian, typical values for limestone were used when no specific reservoir information was available. For the Dinantian limestone a Young's modulus of 40 GPa and a Poisson's ratio of 0.2 were used according to the value for the Carboniferous in Lele et al. (2015). According to Schmitt (2015) the solid bulk moduli of Calcite and Dolomite are 73.3 GPa and 94.9 GPa, respectively. Assuming a calcite dominated limestone, we use a value of 80 GPa. The resulting drained bulk modulus and Biot coefficient are 22.2 GPa and 0.72, respectively (Table 22).

Table 22: Elastic properties of all model units.

Model property	Limburg (claystone)	Dinantian (limestone)	Devonian (clst/sst)
Young's modulus (GPa)	40 <sup>1</sup>	40 <sup>1</sup>	25
Poisson's ratio (-)	0.2 <sup>1</sup>	0.2 <sup>1</sup>	0.2
Solid bulk modulus (GPa)	50 <sup>3</sup>	80 <sup>2</sup>	45
Drained bulk modulus* (GPa)	22.2	22.2	13.9
Biot coefficient* (-)	0.56	0.72	0.69

<sup>1</sup>Lele et al. (2015), <sup>2</sup>Schmitt (2015), <sup>3</sup>Delage (2013), \*calculated

### 3.1.4. Hydraulic properties

The Dinantian is a low porosity and low permeability limestone formation. Similar or even lower values can be expected for the top and bottom layers (Table 23). Flow is governed by fracture flow.

Table 23: Hydraulic properties of all model units.

Model property	Limburg (claystone)	Dinantian (limestone)	Devonian (clst/sst)
Hor. permeability (mD)	0.001	1 (<0.01-2) <sup>1</sup>	0.001
Hor./vert. permeability (-)	1	1	1
Porosity (%)	1	2 <sup>2</sup> (0.5-5) <sup>3</sup>	1

<sup>1</sup>Reijmer et al. (2017), <sup>2</sup>van Hulst and Poty (2009), <sup>3</sup>Carlson et al. (2019)

### 3.1.5. Thermophysical properties

The description of the Limburg properties can be found in the respective sections on the Slochteren model. The Devonian properties are an approximate average of claystone and sandstone and thus correspond to the Alblasserdam Member as defined above. For the Dinantian, typical values for limestone were used when no specific reservoir information was available. According to Fuchs et

al. (2015), Calcite and Dolomite have a thermal conductivity of 3.4 and 5.4 W/m/°C, a heat capacity of 820 and 870 J/kg/°C, and a density of 2710 and 2880 kg/m<sup>3</sup>, respectively. We use values closer to the ones of Calcite. Srinivasan (1955) report similar values of thermal expansion coefficient for calcite and for quartz. Therefore, we use the same value of 30 1e-6/°C for the Dinantian limestone and for the Slochteren Sandstone (Table 24).

*Table 24: Thermophysical properties of all model units. Values refer to rock matrix values unless otherwise stated.*

<b>Model property</b>	<b>Limburg (claystone)</b>	<b>Dinantian (limestone)</b>	<b>Devonian (clst/sst)</b>
Solid thermal conductivity (W/m/°C)	2.0 <sup>4</sup> (1.8-2.7) <sup>2</sup>	3.5 <sup>2</sup>	2.5 <sup>8</sup>
Solid heat capacity (J/kg/°C)	860 <sup>3</sup> (840 <sup>1</sup> -870 <sup>4</sup> )	830 <sup>2</sup>	860 <sup>3</sup>
Volumetric bulk thermal expansion coefficient (1e-6/°C)	30 (15 <sup>7</sup> -50) <sup>6</sup>	30 <sup>16</sup>	30 (15 <sup>7</sup> -50) <sup>6</sup>
Solid density (kg/m <sup>3</sup> )	2650 <sup>5</sup> (2000-3000) <sup>5</sup>	2750 <sup>2</sup>	2650 <sup>5,8</sup>

<sup>1</sup>Daniilidis et al. (2016), <sup>2</sup>Fuchs et al. (2015), <sup>3</sup>Waples and Waples (2004), <sup>4</sup>Doddema (2012), <sup>5</sup>Blake (2008), <sup>6</sup>McTigue (1986), <sup>7</sup>Zhang et al.(2007), <sup>8</sup>Willems et al. (2020)

### 3.1.6. Fault properties

Fracture apertures based on FMI logs in the Dinantian carbonates, were approximately 170 µm (Broothaers et al., 2019; Leverink and Geel, 2019). Assuming this fracture aperture to be equivalent to the hydraulic aperture and the cubic law, this yields a fracture permeability of 1000 mD. Thus, we use the same fault properties as in the Slochteren model except for a higher fault permeability of 1000 mD, a correspondingly higher aperture of 110e-6 m and a higher fault porosity of 100%. The same parameters were used for hydraulic fracture properties (Table 25).

*Table 25: Fault and hydraulic fracture properties. Faults are represented as 2D surfaces without damage zone. Permeability is assumed to be independent of direction and faults are assumed to be filled to 100% with water. Thermophysical fault properties thus correspond to the properties of water.*

<b>Model property</b>	<b>Limburg (claystone)</b>	<b>Dinantian (limestone)</b>	<b>Devonian (clst/sst)</b>
Fault friction coefficient (-)	0.6 (0.7) <sup>1,2</sup>	0.6 <sup>1,2</sup> (0.5-0.7) <sup>1</sup>	0.6 (0.5) <sup>1,2</sup>
Fault cohesion (MPa)	0	0	0
Fault aperture (m)	110e-6	110e-6	110e-6

Fault permeability (mD)	1000	1000	1000
Fault porosity (%)	100	100	100
RSF a-value (-)	0.005 <sup>1</sup> (0.001 – 0.03) <sup>1</sup>	0.005 <sup>1</sup> (0.001 – 0.03) <sup>1</sup>	0.005 <sup>1</sup> (0.001 – 0.03) <sup>1</sup>
RSF b-value (-)	0.0025 <sup>1</sup> (-0.006 – 0.03) <sup>1</sup>	0.0025 <sup>1</sup> (-0.006 – 0.03) <sup>1</sup>	0.0025 <sup>1</sup> (-0.006 – 0.03) <sup>1</sup>
RSF (a-b)-value (-)	0.0025 <sup>1</sup> (-0.003 – 0.012) <sup>1</sup>	0.0025 <sup>1</sup> (-0.003 – 0.012) <sup>1</sup>	0.0025 <sup>1</sup> (-0.003 – 0.012) <sup>1</sup>
RSF critical slip distance d <sub>c</sub> (mm)	1e-5 <sup>1</sup> (2e-6 – 3e-4) <sup>1</sup>	1e-5 <sup>1</sup> (2e-6 – 3e-4) <sup>1</sup>	1e-5 <sup>1</sup> (2e-6 – 3e-4) <sup>1</sup>

<sup>1</sup>Hunfeld et al. (2017, 2020), <sup>2</sup>Buijze et al. (2017)

### 3.1.7. Reservoir fluid data

No fluid information is available for the deep Dinantian limestone formation. We thus use high salinity fluid of the Groß Schönebeck reservoir as formation fluid (Table 26). This is the same as in the Slochteren model.

*Table 26: Pure water properties and hypothetical reservoir fluid based on the Groß Schönebeck Rotliegend water properties for pressure and temperature conditions found at injection well (30°C and 30 MPa) and production well (80°C and 20 MPa). Additionally, the properties for the base case model and sensitivity analysis are summarized.*

Model property	H2O at 30°C and 30 MPa	H2O at 80°C and 20 MPa	GrSk fluid at 30°C and 30 MPa	GrSk fluid at 80°C and 20 MPa	Base case model	Sensitivity
Density (kg/m <sup>3</sup> )	1009 <sup>1</sup>	980 <sup>1</sup>	1185 <sup>2</sup>	1154 <sup>2</sup>	f(P/T) <sub>GrSk</sub>	-
Viscosity (mPas)	0.80 <sup>1</sup>	0.36 <sup>1</sup>	1.51 <sup>2</sup>	0.68 <sup>2</sup>	f(P/T) <sub>GrSk</sub>	-
Volumetric thermal expansion coefficient (1/°C)	3.27e-4 <sup>1</sup>	6.21e-4 <sup>1</sup>	4.10e-4 <sup>3,*</sup>	5.40e-4 <sup>3,*</sup>	-	-
Specific heat capacity	4106 <sup>1</sup>	4156 <sup>1</sup>	3227 <sup>2</sup>	3248 <sup>2</sup>	3240	-

(J/kg/°C)						
Thermal conductivity (W/m/°C)	0.629 <sup>1</sup>	0.680 <sup>1</sup>	0.595 <sup>4,*</sup>	0.649 <sup>4,*</sup>	0.625	-
Bulk modulus (GPa)	2.41 <sup>1</sup>	2.30 <sup>1</sup>	3.70 <sup>2</sup>	3.41 <sup>2</sup>	3.4	-

<sup>1</sup>Lemmon et al. (2018), <sup>2</sup>Francke et al. (2013), <sup>3</sup>Rogers and Pitzer (1982), <sup>4</sup>Aleksandrov et al. (2013), \*value for 5mol NaCl solution, GrSk=Groß Schönebeck

### 3.1.8. Operational and wellbore data

Operational and wellbore data (Table 27) is the same as in the other two models except that for one scenario, the two deviated wells are 1000 m apart and intersect the fault; and in another scenario two horizontal wells parallel to the minimum horizontal stress direction are 500 m apart and hydraulically connected by 5 hydraulic fractures with a spacing of 200 m. The distance between wells and fault is here 250 m.

Table 27: Operational and wellbore data. Operations are typically year-round (up to 8670 hr/a; Mijnlief, 2020). Two scenarios are considered: a) inclined wells intersect the fault and b) horizontal wells with multiple parallel hydraulic fractures are placed next to the fault.

Model property	Value
Distance between wells and fault (m)	0 / 250
Well spacing (m)	1000 / 500
Well inclination from vertical (°)	45 / 90
Re-injection temperature (°C)	30 <sup>2,3,4</sup> (15-45)
Flow rate (l/s)   Flow rate (m <sup>3</sup> /hr)	70 (30 <sup>1</sup> -100 <sup>1</sup> )   ~250 (~110 <sup>1</sup> ~350 <sup>1</sup> )
Length of perforated/open interval (m)	Throughout the reservoir unit
Wellbore diameter (inch)	8 1/2

<sup>1</sup>Mijnlief (2020), <sup>2</sup>Hurter and Schellschmidt, 2003, <sup>3</sup>Wang et al., 2019, <sup>4</sup>Willems et al., 2017

### 3.2. Modeling scenarios

Three models are setup for the Dinantian reservoir (Table 28). Due to the low reservoir

permeability geothermal exploitation needs to focus on existing fault zones (Scenarios S39 and S40) or stimulated fractures (Scenario S41).

Table 28: Summary of specific modeling scenarios for the Dinantian limestone reservoir.

Scenario ID	Description	Changed values
S39	Dinantian fault model (Figure 4)	Wells intersect fault
S40	Dinantian fault damage zone model (Figure 5)Bu	50 m damage zone with same properties as the fault is added on each side of the fault
S41	Dinantian EGS model (Figure 6)	Parallel horizontal wells intersected by parallel hydraulic fractures

## References

Aleksandrov, A.A., Dzhuraeva, E.V., Utenkov, V.F. (2013): Thermal conductivity of sodium chloride aqueous solutions, *Thermal Engineering* 60(3):190-194.

<https://doi.org/10.1134/S0040601513030026>

Apelblat, A., Manzurola, E. (1999): Volumetric properties of water, and solutions of sodium chloride and potassium chloride at temperatures from  $T = 277.15 \text{ K}$  to  $T = 343.15 \text{ K}$  at molalities of (0.1, 0.5, and 1.0)  $\text{mol} \cdot \text{kg}^{-1}$ . *J. Chem. Thermodynamics* 31:869-893.

<https://doi.org/10.1006/jcht.2000.0771>

Blackwell D, Steele J. Heat flow and geothermal potential of Kansas. *Biul Kans Geol Surv.* 1989;226:267–95.

Blake G.R. (2008) Particle density. In: Chesworth W. (eds) *Encyclopedia of Soil Science. Encyclopedia of Earth Sciences Series.* Springer, Dordrecht. [https://doi.org/10.1007/978-1-4020-3995-9\\_406](https://doi.org/10.1007/978-1-4020-3995-9_406)

Blöcher, G., Cacace, M., Jacquy, A. B., Zang, A., Heidbach, O., Hofmann, H., Kluge, C., Zimmermann, G. (2018): Evaluating Micro-Seismic Events Triggered by Reservoir Operations at the Geothermal Site of Groß Schönebeck (Germany). - *Rock Mechanics and Rock Engineering*, 51, 10, 3265-3279.

<https://doi.org/10.1007/s00603-018-1521-2>

Blöcher, M.G., Zimmermann, G., Moeck, I., Brandt, W., Hassanzadegan, A., Magri, F. (2010): 3D numerical modelling of hydrothermal processes during the lifetime of a deep geothermal reservoir. *Geofluids* 10:406-421. <https://doi.org/10.1111/j.1468-8123.2010.00284.x>

Britannica: <https://www.britannica.com/science/rock-geology/Thermal-properties>

Buijze, L., van den Bogert, P.A.J., Wassing, B.B.T., Orlic, B., ten Veen, J. (2017): Fault reactivation mechanisms and dynamic rupture modelling of depletion-induced seismic events in a Rotliegend gas reservoir. Netherlands Journal of Geosciences – Geologie en Mijnbouw 96(5):131-148. <https://doi.org/10.1017/njg.2017.27>

Carlson, T. (2019). Petrophysical Report of the Dinantian Carbonates in the Dutch Subsurface. SCAN report. <https://www.nlog.nl/sites/default/files/2020-11/SCAN%20Dinantien%20Petrophysical%20Report%20of%20the%20Dinantian%20Carbonates%20in%20the%20Dutch%20Subsurface.pdf>

Daniilidis, A., Doddema, L., Herber, R. (2016): Risk assessment of the Groningen geothermal potential: From seismic to reservoir uncertainty using a discrete parameter analysis. Geothermics 64:271-288. <http://dx.doi.org/10.1016/j.geothermics.2016.06.014>

Delage, P. (2013): On the thermal impact on the excavation damaged zone around deep radioactive waste disposal. International Journal of Rock Mechanics and Geotechnical Engineering 5:179-190. <http://dx.doi.org/10.1016/j.jrmge.2013.04.002>

De Jager, J. (2007): Geological development. Geology of the Netherlands Edited by Th.E. Wong, D.A.J. Batjes & J. de Jager. Royal Netherlands Academy of Arts and Sciences, 2007: 5–26

Doddema, L. (2012). The influence of reservoir heterogeneities on geothermal doublet performance. Master Thesis. University of Groningen.

Duin, E.J.T., Doornenbal, J.C., Rijkers, R.H.B., Verbeek, J.W., Wong, T.E. (2006): Subsurface structure of the Netherlands – results of recent onshore and offshore mapping. Netherlands Journal of Geosciences – Geologie en Minjbouw 85(4):245-276. <https://doi.org/10.1017/S0016774600023064>

Evans Jr., H.T. (1979): The thermal expansion of Anhydrite to 1000°C. Phys. Chem. Minerals 4:77-82. <https://doi.org/10.1007/BF00308361>

Falzone, A.J., Stacey, F.D. (1982): Measurements of thermal expansions of small mineral crystals. Phys. Chem. Minerals 8:212-217.

Francke, H, Kraume, M., Saadat, M. (2013): Thermal-hydraulic measurements and modelling of the brine circuit in a geothermal well. Environmental Earth Sciences 70:3481-3495. <http://dx.doi.org/10.1007/s12665-013-2612-8>

Fuchs, S., Balling, S. Förster, A. (2015). Calculation of thermal conductivity, thermal diffusivity and specific heat capacity of sedimentary rocks using petrophysical well logs, Geophysical Journal International 203(3):1977–2000, <https://doi.org/10.1093/gji/ggv403>

Ghabezloo S, Sulem J. Stress dependent thermal pressurization of a fluid-saturated rock. Rock Mech Rock Eng 2008;42:1–24. <https://doi.org/10.1007/s00603-008-0165-z>

Griffith, J., 1936. Thermal expansion of typical American rock. Iowa State College of Agriculture and Mechanics Arts. Iowa Engineering Experiments 35 (19), 24.

Guises, R., Embry, J.-M., Barton, C. (2015): Dynamic Geomechanical Modelling to Assess and Minimize the Risk for Fault Slip during Reservoir Depletion of the Groningen Field. Baker Hughes project report for NAM, project reference: NAM0001, Revision No. 1, June 2015.

Hassanzadegan, A., Blöcher, G., Zimmermann, G., Milsch, H. (2012): Thermoporoelastic properties of Flechtinger sandstone. International Journal of Rock Mechanics and Mining Sciences 49:94-104. <https://doi.org/10.1016/j.ijrmms.2011.11.002>

Van Hulten, F.F.N., Poty, E. (2009). Dinantian Reefs underneath the Netherlands. 71st EAGE Conference and Exhibition. <https://doi.org/10.3997/2214-4609.201400477>

Hurter, S., Schellschmidt, R. (2003): Atlas of geothermal resources in Europe. Geothermics 32(4-6):779-787. [https://doi.org/10.1016/S0375-6505\(03\)00070-1](https://doi.org/10.1016/S0375-6505(03)00070-1)

Hunfeld, L.B., Chen, J., Hol, S., Niemeijer, A.R., Spiers, C.J. (2020): Healing behaviour of simulated fault gouges from the Groningen gas field and implications for induced fault reactivation. Journal of Geophysical Research Solid Earth 125(7):e2019JB018790. <https://doi.org/10.1029/2019JB018790>

Hunfeld, L.B., Niemeijer, A.R., Spiers, C.J. (2017): Frictional properties of simulated fault gouges from the seismogenic Groningen gas field under in situ P-T-Chemical conditions. Journal of Geophysical Research Solid Earth 122(11):8969-8989. <https://doi.org/10.1002/2017JB014876>

Jacquey, A. B., Cacace, M. (2017): GOLEM, a MOOSE-based application v1.0. <https://doi.org/10.5281/zenodo.999400>

Kansy, A. (2007): Einfluss des Biot-Parameters auf das hydraulische Verhalten von Steinsalz unter der Berücksichtigung des Porendrucks. TU Clausthal, Fakultät für Energie- und Wirtschaftswissenschaften, Dissertation. Clausthal.

Kirk, S.S., Williamson, D.M. (2012): Structure and thermal properties of porous geological materials. AIP Conference Proceedings 1426:867. <https://doi.org/10.1063/1.3686415>

Lele, S.P., Garzon, J.L., Hsu, S.-Y., DeDontney, N.L., Searles, K.H., Sanz, P.F. (2015): Groningen 2015 Geomechanical analysis. NAM report, November 2015.

Lemmon, E.W., Bell, I.H., Huber, M.L., McLinden, M.O. (2018). NIST Standard Reference Database 23: Reference Fluid Thermodynamic and Transport Properties-REFPROP, Version 10.0, National Institute of Standards and Technology, Standard Reference Data Program, Gaithersburg.

Van Leverink, D., Geel, K. (2019): Fracture characterization of the Dinantian carbonates in the Dutch subsurface. Report by SCAN, November 2019.

Luo, X., Were, P., Liu, J., Hou, Z. (2015): Estimation of Biot's effective stress coefficient from well logs. *Environmental Earth Sciences* 73:7019-7028. <https://doi.org/10.1007/s12665-015-4219-8>

Malkowski, P., Kaminski, P., Skrzypowski, K. (2012): Impact of heating of Carboniferous rocks on their mechanical parameters. *AGH Journal of Mining and Geoengineering* 36(1):231-241.

McTigue DF (1986) Thermoelastic response of fluid-saturated porous rock. *J Geophys Res* 91(B9): 9533–9542. <https://doi.org/10.1029/JB091iB09p09533>

Mechelse, E. (2017): The in-situ stress field in the Netherlands: Regional trends, local deviations and an analysis of the stress regimes in the northeast of the Netherlands. Master Thesis, TU Delft.

Mijnlieff, H.F. (2020): Introduction to the geothermal play type and reservoir geology of the Netherlands. *Netherlands Journal of Geosciences* 99(e2). <https://doi.org/10.1017/njg.2020.2>

Milsch, H., Regenspurg, S. (2018): Geothermische Fluide als Energieträger und Rohstoffquelle – Herausforderungen und Chancen. - bbr - Fachmagazin für Brunnen- und Leitungsbau, 11, pp. 64—69.

Missal, C.P. (2019): Numerisches Modell zur Entwicklung der Permeabilität von Steinsalz in Abhängigkeit von Schädigung, Fluiddruck und Spannungszustand.

Mohammed, A.K.A. A review: controls on sandstone permeability during burial and its measurements comparison—example, Permian Rotliegend Sandstone. *Model. Earth Syst. Environ.* 6, 591–603 (2020). <https://doi.org/10.1007/s40808-019-00704-w>

Monfared, M., Sulem, J., Delage, P. et al. A Laboratory Investigation on Thermal Properties of the Opalinus Claystone. *Rock Mech Rock Eng* 44, 735 (2011). <https://doi.org/10.1007/s00603-011-0171-4>

Palciauskas, V.V. and Domenico, P.A.: Characterization of drained and uncrained response of thermally loaded repository rocks (1982). *Water Resources Research*. <https://doi.org/10.1029/WR018i002p00281>

Pijnenburg, R.P.J., Verberne, B.A., Hangx, S.J.T., Spiers, C.J. (2019): Inelastic deformation of the Slochteren Sandstone: Stress-Strain Relations and Implications for Induced Seismicity in the Groningen Gas Field. *Journal of Geophysical Research Solid Earth* 124(5):5254-5282. <https://doi.org/10.1029/2019JB017366>

Plevová, E., Vaculiková, L., Kozusníková, A., Danek, T., Pleva, M., Ritz, M., Martynková, G.S. (2011): Thermal study of sandstones from different Czech localities. *J Therm Anal Calorim* 103:835-843. <https://doi.org/10.1007/s10973-010-1129-6>

Reijmer, J., Ten Veen, J., Jaarsma, B., & Boots, R. (2017). Seismic stratigraphy of Dinantian

carbonates in the southern Netherlands and northern Belgium. *Netherlands Journal of Geosciences*, 96(4), 353-379. <https://doi.org/10.1017/njg.2017.33>

Robertson, E.C. (1988): Thermal properties of Rocks. Open-File Report 88-441. <https://pubs.usgs.gov/of/1988/0441/report.pdf>

Schmitt, D.R. (2015): 11.03 - Geophysical Properties of the Near Surface Earth: Seismic Properties, Editor Gerald Schubert, *Treatise on Geophysics (Second Edition)*, Elsevier, pp. 43-87, ISBN 9780444538031, <https://doi.org/10.1016/B978-0-444-53802-4.00190-1>.

Sippel, J., Fuchs, S., Cacace, M., Braatz, A., Kastner, O., Huenges, E., Scheck-Wenderoth, M. (2013): Deep 3D thermal modelling for the city of Berlin (Germany). *Environ Earth Sci* 70:3545–3566. <https://doi.org/10.1007/s12665-013-2679-2>

Skinner, B.J. (1966). Thermal expansion. *Geol. Soc. Am. Mem.* 97:75-96.

Slizowski, J., Nagy, S., Burliga, S., Serbin, K., Polanski, K. (2015): Laboratory investigations of geotechnical properties of rock salt in Polish salt deposits. Mechanical behavior of salt VIII : Proceedings of the Conference on Mechanical Behavior of Salt, SALTMECH VIII : Rapid City, USA, 26–28 May 2015 / eds. Lance Roberts, Kirby Mellegard, Frank Hansen. — Boca Raton, [etc.] : CRC Press Taylor & Francis Group, cop. 2015. — ISBN: 978-1-138-02840-1 ; e-ISBN: 978-1-315-67885-6. — p. 33–38.

Srinivasan, R. The thermal expansion of calcite from room temperature up to 400°C. *Proc. Indian Acad. Sci.* 42, 81–85 (1955). <https://doi.org/10.1007/BF03053495>

TNO-GSN (2021a). Zechstein Group. In: *Stratigraphic Nomenclature of the Netherlands*, TNO – Geological Survey of the Netherlands. Accessed on 28-02-2021 from <http://www.dinoloket.nl/en/stratigraphic-nomenclature/zechstein-group>.

TNO-GSN (2021b). Limburg Group. In: *Stratigraphic Nomenclature of the Netherlands*, TNO – Geological Survey of the Netherlands. Accessed on 28-02-2021 from <http://www.dinoloket.nl/en/stratigraphic-nomenclature/limburg-group>.

TNO-GSN (2021c). Alblasserdam Member. In: *Stratigraphic Nomenclature of the Netherlands*, TNO – Geological Survey of the Netherlands. Accessed on 03-08-2021 from <http://www.dinoloket.nl/en/stratigraphic-nomenclature/alblasserdam-member>.

TNO (2015): Integrated pressure information system for the onshore and offshore Netherlands. Final report. 83 pages.

Trautwein U (2005) Poroelastische Verformung und petrophysikalische Eigenschaften von Rotliegend Sandsteinen. Doctor dissertation, Technische Universität Berlin

Urquhart, A., Bauer, S. (2015): Experimental determination of single-crystal halite thermal conductivity, diffusivity and specific heat from –75 °C to 300 °C. *International Journal of Rock Mechanics and Mining Sciences* 78:350-352. <https://doi.org/10.1016/j.ijrmm.2015.04.007>

Veldkamp, J.G., Goldberg, T.V., Bressers, P.M.M.C., Wilschut, F. (2016): Corrosion in Dutch geothermal systems. TNO report R10160, 15 March 2016, p. 105.

Verweij, J.M., Boxem, T.A.P., Nelskamp, S. (2016): 3D spatial variation in vertical stress in on- and offshore Netherlands; integration of density log measurements and basin modeling results, *Marine and Petroleum Geology* 78:870-882, <https://doi.org/10.1016/j.marpetgeo.2016.06.016>.

Verweij, J., Simmelink, H., Underschultz, J., & Witmans, N. (2012). Pressure and fluid dynamic characterisation of the Dutch subsurface. *Netherlands Journal of Geosciences - Geologie En Mijnbouw*, 91(4), 465-490. <https://doi.org/10.1017/S0016774600000342>

Wang, Y., Khait, M., Voskov, D., Saeid, S., Bruhn, D. (2019): Benchmark test and sensitivity analysis for Geothermal Applications in the Netherlands. Proceedings of the 44th Workshop on Geothermal Reservoir Engineering, Stanford University, Stanford, California, February 11-13, SGP-TR-214.

Waples, D.W., Waples, J.S. (2014): A Review and Evaluation of Specific Heat Capacities of Rocks, Minerals, and Subsurface Fluids. Part 1: Minerals and Nonporous Rocks. *Natural Resources Research* 13(2):97-122. <https://doi.org/1520-7439/04/0600-0097/1>

Willems, C.J.L., Nick, H.M., Weltje, G.J., Bruhn, D.F. (2017): An evaluation of interferences in heat production from low enthalpy geothermal doublet systems. *Energy* 135:500-512. <https://doi.org/10.1016/j.energy.2017.06.129>

Willems, C., Vondrak, A., Mijnlief, H., Donselaar, M., & Van Kempen, B. (2020). Geology of the Upper Jurassic to Lower Cretaceous geothermal aquifers in the West Netherlands Basin – an overview. *Netherlands Journal of Geosciences*, 99, E1. <https://doi.org/10.1017/njg.2020.1>

Yoon, J.-S., & Zang, A. (2019). 3D Thermo-Mechanical Coupled Modelling of Thermo-Seismic Response of a Fractured Rock Mass related to the Final Disposal of Spent Nuclear Fuel and Nuclear Waste in Hard Rock. Swedish Radiation Safety Authority SSM Report 2019:15.

Zang, A., Wagner, C.F., Dresen, G. (1996): Acoustic emission, microstructure, and damage model of dry and wet sandstone stressed to failure. *Journal of Geophysical Research Solid Earth* 101(B8):17507-17521. <https://doi.org/10.1029/96JB01189>

Zhang, D., Jeannin, L., Hevin G., Egermann, P., Potier, L., Skoczylas, F. (2018): Is salt a poro-mechanical material? 52nd US Rock Mechanics / Geomechanics Symposium, Seattle, Washington, USA, 17-20 June 2018. ARMA 18-0423.

Zhang, C.-L., Rothfuchs, T., Jockwer, N., ..., Komischke, M. (2007): Thermal Effects on the Opalus Clay. Final Report. GRS – 224, ISBN 978-3-931995-98-0. [https://www.grs.de/sites/default/files/pdf/grs-224\\_0.pdf](https://www.grs.de/sites/default/files/pdf/grs-224_0.pdf)

Zimmerman, R.W. (2000): Coupling in poroelasticity and thermoelasticity. *Int J RockMech Min Sci* 37(1–2):79–87. <https://doi.org/10.1016/j.ijrmms.2011.11.002>

Zoback, M.D., 2007. Reservoir Geomechanics: Earth Stress and Rock Mechanics Applied to Exploration, Production and Wellbore Stability. Cambridge University Press.